2009

DESIGN AND DEVELOPMENT OF A PVDF SENSOR TO MONITOR INTRACRANIAL PRESSURE (ICP)

VIVEK VIJAYWARGI
Virginia Commonwealth University

DESIGN AND DEVELOPMENT OF A PVDF SENSOR TO MONITOR INTRACRANIAL PRESSURE (ICP)

A thesis submitted in partial fulfillment of the requirements for the degree of Master of Science in Engineering at Virginia Commonwealth University.

by

VIVEK VIJAYWARGI
B. Tech., Jawahar Lal Nehru Technology University-Hyderabad, India 2007

Director: DR. KARLA M. MOSSI
ASSOCIATE PROFESSOR, MECHANICAL ENGINEERING

Virginia Commonwealth University
Richmond, Virginia
May 2010

Acknowledgement

It's been a challenging and great experience for the achievement of this Masters degree. I do not alone take the credit for this achievement; I would like to thank the most important person Professor Dr. Karla M. Mossi for her invaluable support and knowledge. I personally want to thank her for never ending patience and encouragement. Her assistance, support and guidance were always available. She was the backbone of this project and her innovative ideas led to easy and smooth completion of this study. She was a great mentor and always had an awesome smile on her face. I cannot thank her enough for her mentorship.

Deepest gratitude are also due to the members of the supervisory committee, Dr. Ramana M Pidaparti, Dr. Kevin R Ward and Dr. Martin L Lenhardt without whose knowledge and assistance this study would have not been successful. During the course of my research work, the professional expertise and support of the following have been instrumental in attaining the desired outcomes. Dr. Pidaparti always had a vision for ideas and innovations and the way he potrayed was of great help. Would like to thank Dr. Lenhardt and Dr.Ward who took time out from their busy schedule to be a part of my committee. Your suggestions were most useful and helped me a lot in understanding the concepts better.

Special thanks to Poorna Mane, Ravi Bhadauria, Jugal Kapadia and Shyam Bhardawaj. They were asset to me as friends and were always present when I needed their guidance. In particular Poorna who had a lot of experience with the materials and equipments, she was an unwavering support to me. Her mood was always light and joyous never got angry on my mistakes. The fellow students in lab Jingi Xie, Patrick Proffitt, Matthew Richeson and Rami Hijaz were of great help, special thanks to them also. Patrick and Rami helped me a lot in making leads, sensors and testing them. My friends Shilpa, Suditi, Priyanka, Sahil and many more thanks for partying with me and bearing all my tantrums and talks.

My parents and family was always with me, especially me sister who has always pushed and guided me for a better performance.

Table of Contents

Page

List of Figures

Page

List of Tables

Page

Abstract

DESIGN AND DEVELOPMENT OF A PVDF SENSOR TO MONITOR

INTRACRANIAL PRESSURE (ICP)

By Vivek Vijaywargi, M.S.

A Thesis submitted in partial fulfillment of the requirements for the degree of Master of Science in Engineering at Virginia Commonwealth University.

Virginia Commonwealth University, 2010

Major Director: Dr. Karla M. Mossi
Associate Professor, Mechanical Engineering

The brain is surrounded by cerebrospinal fluid, and when a brain tumor or a traumatic brain injury has occurred, intracranial pressure, ICP, is developed. Monitoring ICP non-invasively is a challenge. Currently, a probe is inserted through the skull, running the risk of infection, bleeding, and damage to the brain tissue with residual neurologic effects. A novel method to measure ICP using actuators and sensors has been proposed where the skull is vibrated at high frequencies and the receiving signal is measured at the surface eyelid. A design of experiments approach is used to develop the sensor part of the

ICP monitoring device so that gain can be maximized using factors such as area, thickness, electrode, and applied pressure. A full factorial statistical model with 4 factors and at different levels with 2 replicates was developed, each factors had 2 levels except area, which had 5 levels. A total of 120 samples were manufactured and tested.

Statistical analysis showed that thickness has the biggest effect on overall gain. However, combination of all other factors cannot be ignored when maximizing gain. For instance, thicker samples of 110μm had an average gain of -39dB, at 50 kHz. Numerical analysis confirmed these results.

In addition, sensor packaging is optimized to minimize dampening of the signal and ensure durability, reliability, and repeatability of the measurements. Results of this study showed that for a range of areas and thicknesses with Cu-Ni electrodes packaged with Scotch Packaging super strength 3M are the optimum factors for the ICP sensor. These parameters are then incorporated into a design, the ICP glasses that allow ease of application and consistency of the measurements. The sensitivity of the sensor was measured to be 0.211mV/V.

1 Introduction

Intracranial pressure (ICP) is the pressure exerted on the rigid, bony skull by its constituents that are brain, cerebrospinal fluid (CSF), and the cerebral blood. It is described as pressure exerted by the cranium on the brain tissue, CSF, and the brain's circulating blood volume (Mokri 2001). ICP is a dynamic phenomenon constantly fluctuating in response to activities such as exercise, coughing, straining, arterial pulsation, and respiratory cycle.

Pressure increase in the brain which is encased in skull can lead to serious medical conditions which can be life threatening. Elevated or increased ICP is a serious complication that can result from various neurologic conditions such as head trauma, intracranial hemorrhage, embolic stroke, alterations in cerebral spinal fluid production and/or absorption, infections, and tumors (Josephson 2004).

Patients with increased ICP are among the most challenging patients to care for in a critical care setting. Increased ICP is a medical/surgical emergency. Initiating rapid and effective treatment to protect a patient from a devastating outcome depends on aggressive and thorough clinical assessment (Arbor 2004). ICP is closely related to cerebral perfusion, blood flow in brain. Healthcare professionals should have a solid understanding of the pathophysiology of ICP treating patients with neurologic conditions associated with elevated ICP. The treatment goal to reduce ICP is normally to manipulate, and ultimately

to decrease the volume of one of three components of the intracranial space: blood, brain tissue, or CSF.

Headache and facial edema are commonly observed symptoms in human subjects exposed to both actual weightlessness and weightlessness simulated by a head-down tilt (HDT) (Hargens et al. 1983 and Thornton et al. 1977). Increased ICP may contribute to these symptoms, as well as to the space motion sickness experienced by astronauts. HDT elevates ICP in monkeys (Keil et al. 1991). However, there is no direct evidence that actual weightlessness increases ICP, because there is currently no established method for sensitively, accurately, and non-invasively measuring ICP or changes in ICP in healthy adults.

Neurological damage does not occur immediately at the moment of impact (primary injury) but evolves afterwards (secondary injury). Secondary brain injury is the leading cause of in hospital deaths after traumatic brain injury (TBI) (Marshall et al. 1991). In the United States, TBI is a leading cause of death for persons under age forty-five and occurs every fifteen seconds. An estimated 5.3 million American, approximately 2% of US population, currently live with disabilities resulting from TBI (Thurman et al. 1999). The leading causes of TBI are motor vehicle accidents, falls, and sports injuries, as shown in Figure 1-1.

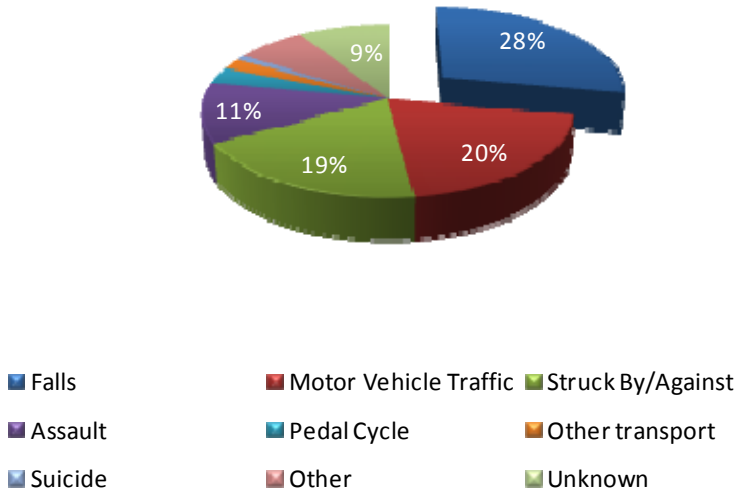

Figure 1-1: Leading causes of TBI (Langlois et al. 2004)

TBI contributes to a substantial number of deaths and cases of permanent disability. Each year in the United States, an estimated:

- 1.4 million people sustain a TBI. Of them, 235,000 are hospitalized and survive (Langlois et al. 2004, Johnson 2001)
- 30% of those evacuated from battlefield to Walter Reed Army Medical Center have TBI (Singer 2008)
- 1.1million people who sustain a TBI are treated and released from an emergency department
- 50,000 people die from a TBI (Langlois et al. 2004)
- 80,000 to 90,000 people experience the onset of long-term or lifelong disability associated with a TBI (Thurman et al. 1999)

Among children ages 0 to 14 years, TBI results in an estimated of 2685 deaths and 435,000 emergency department visits (Langlois et al. 2004). In almost every age group, TBI rates are higher for men than for women and in that almost 75% of TBIs that occur each year are concussions or other forms of mild TBI (CDC 2003). Direct and indirect costs of TBI were an estimated $60 billion in the United States in 2000 (Finkelstein et al. 2006).

Normal ICP in adults ranges from 0-15 mmHg. Typically, sustained ICP levels above 20 mmHg can result in brain injury. It is important to understand that the definition of an elevated ICP depends on the specific pathology. In hydrocephalus for example, a pressure above 15 mmHg can be regarded as high whereas in a head injury, aggressive treatment usually starts at or below 25 mmHg (Czosnyka & Pickard, 2004). ICP can also depart from a "normal range" based on other factors such as age, body posture, and other clinical conditions. ICP is mainly derived from the CSF and cerebral blood circulatory dynamics (two of the three intracranial vault components) (Czosnyka & Pickard, 2004).

The other component of the intracranial vault, the brain tissue, has for the most part, a constant volume. There are times when the volume of the brain tissue can be altered during the presence of a mass lesion or in the setting of edema. ICP is usually more dependent on changes in the volumes of CSF and cerebral blood than as a result of changes in the brain tissue. CSF is produced continuously and is normally reabsorbed into the venous system. Cerebral blood flow (CBF) determines the volume of the cerebral blood in the intracranial vault. The intracranial compartment consists of brain approximately 83%, CSF approximately 11%, and blood approximately 6%. Under normal conditions there are

two main components of ICP, CSF and vasogenic (Czosnyka 2000), it is derived from circulation of CSF and is responsible for ICP. An increase in the volume of one of the components of the intracranical cavity (e.g., brain) requires a compensatory reduction in another (e.g., CSF) to maintain a constant pressure. Brain tissue is essentially incompressible, so any increase in ICP due to brain swelling initially results in extrusion of CSF and blood from intracranial cavity a phenomenon known as spatial compensation. Most secondary brain injury is caused by brain swelling, with an increase in ICP and a subsequent decrease in cerebral perfusion leading to ischaemia (Graham et al. 1989). Within hours of TBI, vasogenic fluid accumulating in brain causes cerebral oedema, raises ICP, and lowers the threshold of systemic blood pressure (DeWitt et al. 1995). A reduction in cerebral blood flow or oxygenation below a threshold value or increased ICP leading to cerebral herniation increases brain damage and morbidity.

Before the early 1980's, most ICP monitors were fluid coupled devices of variable utility and accuracy (Feldman et al. 1993 and Luerssen et al. 1989). The first ICP microtransducers were introduced in the 1980'sby Honeywell Microtransducer Catheter MTC-P5F. It was first designed for intraparenchymal pressure measurement (Ostrup et al. 1987). However, these devices also require the full penetration of the brain, especially in the case of small and shifted ventricles. The subsequent development and now wide spread use of implantable fiberoptic or strain gauge microtransducers has added substantially to Neurosurgeon's ability to safely and accurately measure ICP. The complication rate for these monitors is extremely low, mostly because of the small diameter and the lack of fluid coupling (Pople et al. 1995 and Shapiro et al. 1996). However, these monitoring techniques

are relatively expensive. Breakage or malfunction generally requires complete replacement of the intracranical probe.

Attempts have been made to monitor ICP noninvasively in infants by the application of a variety of fontanel "tonometers." These devices require a certain minimal size of the anterior fontanel, lack of scalp swelling and a high degree of maintenance to obtain accurate readings (Kaiser et al. 1987). These concerns, as well as the limited number of disorders requiring continuous ICP measurements in infants, have limited the interest in and widespread use of fontanel tonometry.

ICP cannot be reliably estimated from any specific clinical feature or computed tomography (CT) finding and must actually be measured. Different methods of monitoring ICP have been developed but selection and the type of ICP monitor should be guided by the clinical presentation and the therapeutic strategy that is chosen for each patient. All current clinical available methods used for measuring ICP are invasive and makes use of various transducer systems, each of them has their advantages and disadvantages. Current ICP monitors allow pressure transduction by external strain gauge, catheter tip strain gauge, or catheter tip fiberoptic technology. External strain gauge transducers are coupled to the patient's intracranial space via fluid-filled lines, whereas catheter tip transducer technologies are placed intracranially. External strain gauge transducers are accurate and can be recalibrated, but obstruction of the fluid couple can cause inaccuracy. The principle of operation of pressure transducers is that the resistance of a wire is inversely proportional to its length; four strain sensitive wires are connected to a wire frame attached to the diaphragm of the transducer. The set of wires form Wheatstone bridge network energized

by direct current. Pressure applied to the transducer diaphgram causes changes in resistance of the strain gauges and thus an imbalance in the bridge circuit. This is detected by an amplifier and the signal displayed on an oscilloscope (Ravi and Morgan 2003).

1.1 Current Techniques

In patients for whom ICP monitoring is indicated, a decision must be made as to what type of monitoring device to be used. The optimal ICP monitoring device is one that is accurate, reliable, and cost effective and causes minimal patient morbidity. Methods in use may make use of fluid coupled systems or an implantable pressure sensor, the fluid coupled system use sensors consisting of a fluid filled catheter or hollow bolt in communication with the lateral ventricle. The sensors are classified as stain gauge type, fiberoptic tip type, and Implantable devices.

1.1.1 Strain gauge catheter type

This transducer tip contains a silicon microchip with diffuse resistant strain gauges. The diaphragm is coated with a thin layer of silicone rubber to insulate the transducer from the environment into which it is placed; the strain gauges are connected via tiny wires that extend through the length of flexible nylon tube to complete a Wheatstone bridge type circuit as discussed above. It has a high delity with a frequency response greater than 10 kHz, which is achieved by the elastic properties of silicon, small overall size of the diaphragm and tiny volumetric displacement under pressure. When this is incorporated into a ventricular catheter, the system allows simultaneous drainage of CSF and ICP

recording. It is flexible, and can be tunneled beneath the scalp, preventing it from being easily broken. Its small size (a nominal outer diameter of 0.7mm for the nylon vent tube and 1.2mm for the transducer case) is an additional advantage, particularly for pediatric patients. The absence of a fluid column precludes dampening by blood clots, debris, or air bubbles. Since irrigation is needed, there is low risk of infection (Gray et al. 1996).

1.1.2 Fiberoptic catheter tip

Fiberoptic transducers can be easily placed through the working channel of the endoscope and have interposed assembly (Vassilyadi et al. 2002). It is characterized as having a low zero drift over long periods of time, very good frequency response, and stable linearity (Bray et al. 1989). A very important advantage is that a pressure-sensitive element is placed in the head, so the risk of infection is minimized. This gives it an advantage over prolonged ICP monitoring, which uses a fluid-filled catheter and an external transducer (Poca et al. 2002).

1.1.3 Implantable devices

ICP monitoring-implantable system with no external connections has obvious advantages. These devices would still act as foreign bodies, but the elimination of skin penetration would minimize the risk of infection. The principal problems associated with these types arise from recalibrated after implantation, increased drift, requires complicated and expensive hardware, and shows a slow dynamic response (Chapman et al. 1984).

Sites of measuring ICP can be classified as epidural, subarachnoid, parenchyma, or intraventricular locations. 'Gold standard' of ICP measurement Intraventricular (Weaver et al. 1982, Yaablon et al. 1993, Gopinath et al. 1995) requires placement of a catheter into the lateral ventricle, the reference point for the external transducer is the foramen of Monroe (surface marking-2 cm above the pterion or midpoint of a line joining the two external auditory meati). It is the simplest, most reliable and accurate system available and has the advantage of allowing drainage of CSF to lower ICP. Disadvantages include high bacterial colonization rates defined as positive CSF or catheter tip culture (1-5% after 3 days, though ventriculitis has not been demonstrated in clinical studies), difficult placement, injury to brain tissue and potential for leaks/blocks in the system.

Complications related to ICP technology

The complications of ICP monitoring are dependent on the type of monitor and the presence of systemic disturbances. ICP monitoring complications include infection, hemorrhage, malfunction, obstruction, and mal-position. Although these complications rarely produce long-term morbidity in patients, they can increase costs by requiring replacement of the monitor, and they can give inaccurate ICP readings. Parenchymal monitoring is associated with a very low complication rate, even in relatively high-risk patients. The use of ventricular catheters for ICP monitoring carries a somewhat higher complication rate, although the benefits derived from the use of these monitors frequently outweigh the additional risk. Ventricular catheters are larger than the parenchymal probes, and proper placement requires complete penetration of the brain and accurate positioning

in the ventricles. The major complication associated with the use of ventricular catheters is infection. Most recent series have reported infection rates under 10% (Holloway et al. 1996 and Luerssen et al. 1991). Malfunction or obstruction in fluid coupled ventricular catheters, subarachnoid bolts, or subdural catheters has been reported as 6.3%, 16%, and 10.5%, respectively (Barlow et al 1985 and North et al. 1986).

Ranking of ICP monitoring Technology

ICP monitoring techniques have been ranked based on their accuracy, stability and ability to drain CSF (Bratton et al 2007).

1. Intraventricular devices—fluid-coupled catheter with an external strain gauge or catheter tip pressure transducer.
2. Parenchymal catheter tip pressure transducer devices.
3. Subdural devices—catheter tip pressure transducer or fluid-coupled catheter with an external strain gauge.
4. Subarachnoid fluid-coupled device with an external strain gauge.
5. Epidural devices.

2 Design Considerations and Motivation

This chapter provides a thorough description of the opportunity and scope of this project. As the PolyVinyli Dene Fluoride (PVDF) sensor is designed for the eyelid, the anatomy of the human eye, i.e. its shape and dimensions, are discussed.

2.1 Motivation

There is a need for a technique that can be used to non-invasively monitor intra cranial pressure (ICP). There is a need for a portable, non-invasive sensor for measuring ICP in victims with traumatic head injury, suitable for use in the battle area and during medical evacuation as well as in hospital conditions. This will allow monitoring to prevent secondary brain damage. Timely identification and treatment of elevated ICP will greatly improve the chances of survival of these patients.

There are three approaches allowing potential access to ICP, the ear, eye, and the movement of the skull. ICP in the brain is directly communicated to both the eye and ear. The eye is more convenient to non-invasively monitor changes in ICP.

Ear monitoring of changes in (CSF) pressure has been attempted but has not resulted in a feasible clinical device. The most successful acoustical approach to date is the

combine measurement of skull vibrational resonance with ultrasonic measurement of blood flow in the main optic artery. This is based on the fact that the optic nerve and its vascular bundle are exposed to ICP because the optic nerve and the nerve sheath have a sleeve of CSF that extends up to the ocular globe. Using the sensor over the eyes capable of exerting pressure over the globe it was determined that pressure in the eye equals ICP when the retinal arterial pulsations stop, acoustic sensors were used on a head band for this study (Ragauskas and Gediminas, 1995). Direct measures of skull vibration by using ultrasonic probes have also been attempted, but with limited success because it is technically complicated, and is not a promising clinical alternative. Eye pressure does correlate with CSF and various approaches have been used since eye pressure assessment is a common opthalmological procedure. Two types of intra ocular pressure measurement have been reported, with varying correlations to ICP. The first is non-contact air tonometry, which measures intra ocular pressure. This technique has produced conflicting results and at best provides only a rough estimate of ICP (Lashutka et al. 2004). IOP was measured in humans using air tonometer (Sheeran et al. 2000) and these values were compared to simultaneously obtained ICP. Although a significant correlation between IOP and ICP were found in patients, there was significant variability of this relationship between patients.

The other reported technique is ophthalmodynometry, which is an aplanatic technique. This technique applies pressure to the cornea and measures the intra ocular arterial pulse wave. Pressure is applied to the corneal surface until the intra ocular arterial

pulse wave (produced by the ophthalmic artery) is obliterated. The pressure at which this happens has been termed intra cranial arterial pressure and some have used this pressure to infer changes in ICP. However, this measure cannot be equated with ICP. There have been previous attempts by other researchers to acoustically measure ICP in animals, but although they have proven the validity of the concept, they have not been practical for portable use in humans (Semmlow and Fisher 1982) observed in young dogs that the response of the head to low-level audible vibrations correlates with ICP elevation. They had used sensors for the skull, and a clear understanding of the resonant frequencies and their significance is not demonstrated. Stevanovic et al. 1995, demonstrated the correlation of audible vibration with ICP in sheep, artificially elevating ICP and monitoring the acoustic signal. However, although their method did not require surgery within the skull cavity, it did require implantation of screws in the skull, making it impractical for a portable system.

In another acoustical approach a 1MHz signal was used to record brain resonances in the third ventricle induced by the heart pulse, stronger signal is the second harmonic, which in turn is used to correlate with ICP (Michaeli and Rappaport 2002). In this approach the ultrasound is simply modulated by the low frequency resonances, recording is susceptible to errors induced by changes in the heart rate and pulse pressure, CSF volume in the third ventricle never the less the results were reasonable estimate of ICP. The problem of the approach may not lie in the utility of the results as reported but the cost and application in the field.

Another approach (Dutton et al. 2002), placed a transducer on the forehead to record the deformation of the skull produced by heart pulse. This is a low frequency displacement under 10 Hz and is based on the acoustic transmission properties of the brain tissue, sensing of the movement takes place on the forehead. A patient with increased ICP exhibits small displacements whereas normal patients had a strong skull displacement. However, this study presents evidence that with higher resonance frequency of the brain and the coupled skull complex will serve more informative and serve to offer more knowledge for searching for the algorithm that will accurately reflect ICP.

Most recently a study reported that increased ICP will alter in a proportional fashion, the emissions from the cochlea in an animal model (Buki et al. 2002). The cochlea is connected to the cerebral spinal fluid system via the cochlear aqueduct. The work of Stevanoic et al. 1995 and Lenhardt et al. (1999, 2002) have explored the response of the head to low audio frequencies and ultrasonic frequencies respectively. The signal used employs wider range of frequencies i.e. 20-60 kHz. Only the attenuation of a calibrated ultrasonic noise applied to the head will be measured as the next part of the study through the developed sensor. This will simplify the response parameters and will yield clinically useable information in the field through an output signal, which converts attenuation in db V (dB Volts) to equivalent pressure.

2.2 Design Consideration

The purpose of the PVDF sensor for this project is to fit on the human eyelid and convert any fluctuations of pressure received through the eye into an electrical usable signal. The radius of curvature (e_ρ) of the eye is approximately 1.27 cm, with a height of approximately 1.5 cm to 2.5 cm and a width of approximately 2.4 cm to 4 cm (Fledelius et al. 1992, Denis et al. 1993 and Insler et al. 1987). As the sensor is recording a high frequency response, it should be designed in such a way that it does not come in contact with the eye socket. The orbit, or eye socket, is a cone-shaped bony cavity that protects the eye, as seen in Figure 2-1. **A**s it is a bone cavity it can alter the signal, which is not desired. Our eyelids protect and lubricate our eyes. Small oil-producing glands line the inner edge of our eyelids. These oils mixed with tears when we blink, keep the eye moist and clean.

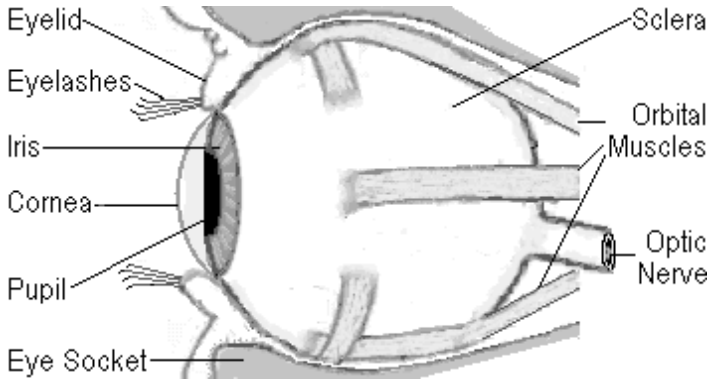

Figure 2-1: Human eye (www.99main.com)

The design considerations for this research project for the development of the sensor is its size and dimensions, provide good response over frequency range as our objective of the study is to develop piezoelectric sensors for measuring acoustic signal, disposable, should be easy to use and portable. Once it's developed, for the testing, repeatable and reliability of signal is desired.

3 Materials and Manufacturing

This chapter describes all parts needed for manufacturing and assembly. The samples are constructed from three main components: the piezoelectric sample itself, electrical leads that conduct the signal, and a protective layer (casing). These components are assembled into a device by following two major steps, (1) Assembly; and (2) Quality assurance described in detail in the following sections.

3.1 Materials

3.1.1 Piezoelectric materials

The term "smart" materials originated in 1880 by Jacques and Pierre Curie with the discovery of piezoelectricity in quartz and Rochelle salt, where the piezoelectric effect is inherent to the material (Jaffe et al. 1971).

Piezoelectric ceramic materials such as Lead Zirconate Titanate (PZT) or zinc oxide are normally preferred as smart material actuators and sensors depending on their polarity and because of their relatively large piezoelectric coefficients (Suplee 1997). However, difficulties in the deposition of thin films and large Young's modulus limit the achievable strain, and their brittle nature has limited their use in a wide range of applications (Wersing et al. 1986). Piezoelectric polymers such as PVDF can overcome some of these difficulties even though they have a relatively low piezoelectric coefficient.

The lower Young's modulus of PVDF facilitates relatively large strain, which can result in large displacements or deflections in the actuators. PVDF materials are available in large sheets of thin film that are easy to shape into specific geometries to implement modal actuators and modal sensors for the control and sensing of flexible structures (Suplee 1997, and Lee 1990) Piezoelectric polymers like PVDF are widely used in sensor elements. Measurement Specialties Inc. supplies a wide range of piezo film sensors made from PVDF film. PVDF is polarized across the thickness of the polymer, which is commercially available in thicknesses of 9, 28, 52, and 110 μm from Measurement Specialist Inc., USA.

3.1.2 Leads

Leads can play an important role in the ease of application of the sensor on the eyelid and also on the comfort level for the patient. Flat metal leads are used to to provide electrical contact to the electrode faces of the PVDF polymer. The leads are Nickel 201 of Wiretronics, (0.001mm x 0.125mm). A constant length of 13 cm was maintained throughout the study. Soldering directly to a PVDF film sheet is difficult since the electrode thickness is small and excessive localized heat damages the sample. As the sensor has to be adjustable on the eyelid it will be easy to use a flat electrode instead of wired.

3.1.3 Shape and Size

Desired shapes can easily be achieved using PVDF film. The human eye is spherical in nature and has a radius of 12.7 mm, so the limitation lies in the area to be covered by the sensor. Since shape may have an effect on the sensitivity of the transducer, 3 different shapes will be considered. As the objective here is to maximize the gain, effect and results of all the shapes will be taken into the design of experiment for the statistical analysis using JMP software. The sensor will be designed and developed so as to cover as much area as possible without touching the orbit. More area is preferred so that a more accurate response can be obtained. The study will be performed so as to quantify the difference in the response (gain) using samples of smaller and larger areas keeping the shape constant. Size of the samples will range from 150 – 300 mm^2. Need more details.

3.1.4 Casing Materials

In order to attach the leads (electrode) to the PVDF sample, packaging material will be used. Its choice will be based on cost, properties, ease of use, and reliability. It will provide a protective shell. Due to the moisture and small dust particles on the eyelid, it should not be slippery. Various kinds of tapes like Furon CHR® Kapton™ adhesive, C-Line self adhesive reinforcing strips (Mylar®), Scotch tape, Scotch Packaging super strength 3M, and Scotch High performance 3M will be tested for this study.

3.2 Assembly

The samples are constructed from three main components: the piezoelectric sample itself, electrical leads that conduct the signal, and a packaging layer. First, one piece of packaging layer is cut to the desired dimensions and laid out, adhesive side up. To that is affixed one of the electrical leads having a shielding layer covering it, followed by the PVDF. The other lead is then placed atop the PVDF, and the final protective layer is laid out, sealing the sample, Figure 3-1shows the schematic of the sensor assembly.

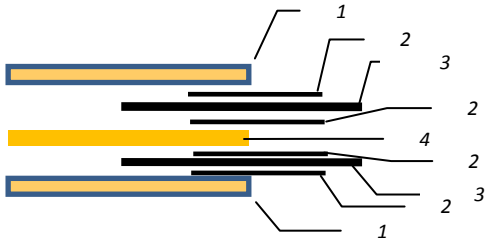

Figure 3-1: Sensor (1) self-adhesive packaging material; (2) flat lead shield; (3) flat conductive lead; (4) sensor material.

3.3 Quality Assurance

All the samples made were tested using a multimeter by checking continuity. Samples that failed this test were discarded. An additional quality test consists of capacitance measurements. Capacitance was measured using a multimeter model FLUKE 189 (at 60Hz) and a Impedance-Gain Phase Analyzer model HP 4194A (100 Hz-60kHz).

Results using the multimeter are shown in Table 3-1. The capacitance values vary from the median by less than 5 percent. Figure 3-2 shows the typical capacitance results at frequencies higher than 100Hz. The trends for all the samples look very similar.

Table 3-1: Capacitance measurement at 60 Hz

Sample number	Capacitance (nF)
1	0.106
2	0.109
3	0.111

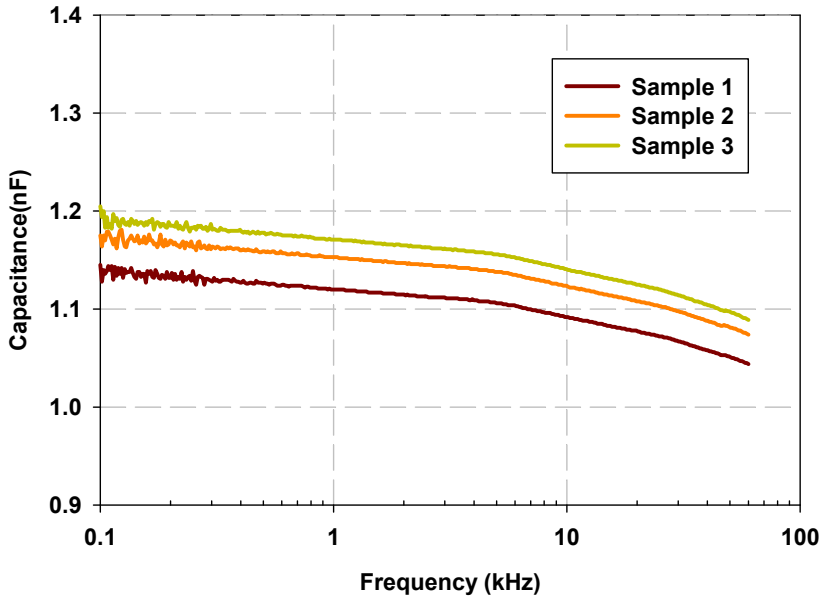

Figure 3-2: Typical capacitance measurement at a range of frequencies of various samples 150 mm^2, with Cu-Ni electrodes and thickness of 110µm

3.4 Peeling Test

In order to ensure the proper packaging of the sensor material different encasing materials were tested. These materials shown in Table 3-2 were chosen because they are commercially available and relatively inexpensive. To test the strength of the bond between sensor (PVDF), leads, and encasing material, a peeling test is conducted with a hand held force probe (Chatillon DPP series -23 model) with a range of 5lbs with a precision of 0.05lbs. Results of these tests are also summarized in Table 3-2. It was observed that High Performance Scotch material (3M) had the highest peeling force of all the materials tested. Gain was measured before the peeling test was performed and the results are shown in Figure 3-3.

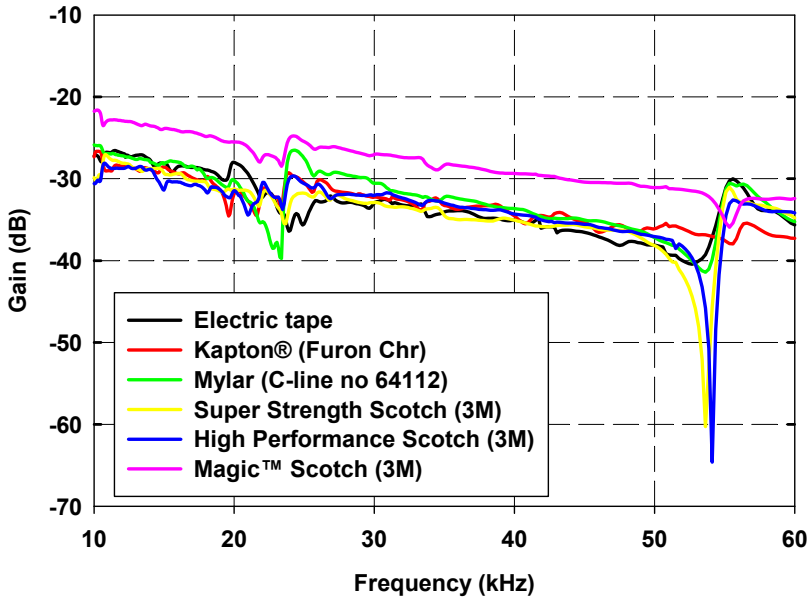

Figure 3-3: Gain measurement with various tapes

Table 3-2: Peeling test results

Packaging material	Lbs
Magic™ Scotch (3M)	1.3
Mylar (C-line no 64112)	1.5
Kapton® (Furon Chr)	1.8
Super Strength Scotch (3M)	2.5
Electric Tape	2.7
High Performance Scotch (3M)	**3.4**

Once all the samples are fabricated and tested individually, their response can then be assessed. These experiments are described in the next chapter.

4 Experimental Setup

This chapter describes the setup used for testing of the samples in the laboratory. The equipment and simulation experiments description is presented here.

4.1 Vibration Source

For ICP monitoring, it has been calculated that the frequency range of vibration required is in the range of 20-60 kHz. Using these parameters, the use of an electromechanical shaker as a vibration source becomes cumbersome. Instead, a piezoelectric Bimorph is chosen as a low vibration source for the frequency range where a response might be detected. Specifically, a Bimorph by Taiheiyo Cement Corporation was used as the actuator for testing purposes in the laboratory. It consists of a multi-layer piezo ceramics plate (PZT), an elastic plate, and electrodes. It had parallel polarization direction and was 60 x 20 x 0.2 mm in size, as seen in Figure 4-1. The device weights approximately 7 grams. The input signal to the Bimorph consisted of a 1V sinusoidal waveform. The output is then acquired with the Impedance-Gain Phase Analyzer.

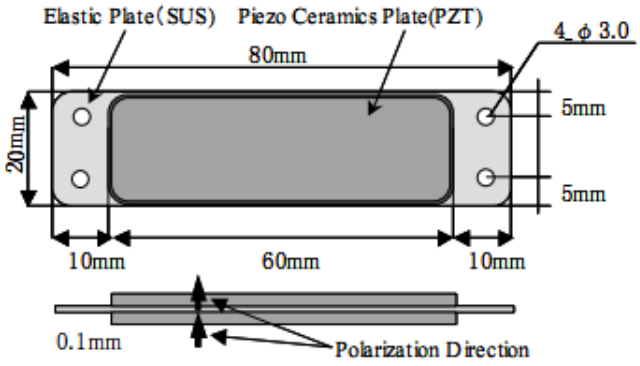

Figure 4-1: Bimorph top view (Eriguchi at al 2008))

4.2 Test Setup

A challenge when using a Bimorph as a vibration source consists on consistent clamping or boundary conditions. To ensure consistent results and reducing variability on the actuator, a setup was developed so as to hold the Bimorph from one end, that is a cantilever beam setup. Clamps were used to hold and adjust the Bimorph without damaging the device. The output channel of the impedance analyzer is connected to the Bimorph (and supply the actuator with a VAC) and the test channel (the input of the impedance analyzer) to the output of the PVDF sensor.

In order to facilitate transmission of any signals from the Bimorph (vibration source) to the sensor (PVDF) several coupling mediums need to be tested**.** The first approach used consisted on using double sided tape. A second approach consisted on adding a pressure (weight) therefore eliminating the need of a coupling or holding mechanism. The final setup is shown in Figure 4-2.

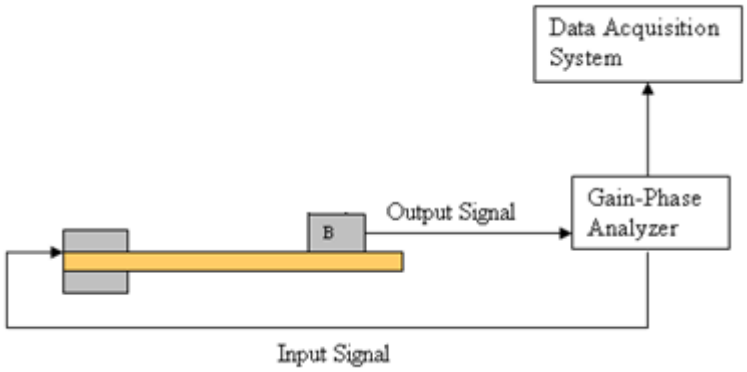

Figure 4-2: Experimental setup schematic, A: Bimorph (Actuator); B: PVDF sensor; C: Clamps

4.3 Calibration

The accelerometer is a standard conventional device used to monitor vibrations in many applications. In order to calibrate the test setup (the bimorph as a vibration source), an accelerometer is utilized to obtain a baseline measurement. Using the setup shown in Figure 4-3(b), a calibration of the setup is performed using an accelerometer 352A60, manufactured by PCB Piezotronics. These results indicate the Bimorph contains vibration peaks at 23, 33, 41 and 55 kHz labeled as A, B, C, and D respectively. Some of these peaks are due to the accelerometer weight on the beam lowering natural resonant an altering the system. However, a similar type of gain and trend should be observed by the PVDF sensor, even though the accelerometer does change the cantilever response due to its own weight (7 grams). The calibration curve shown in Figure 4-3 was obtained.

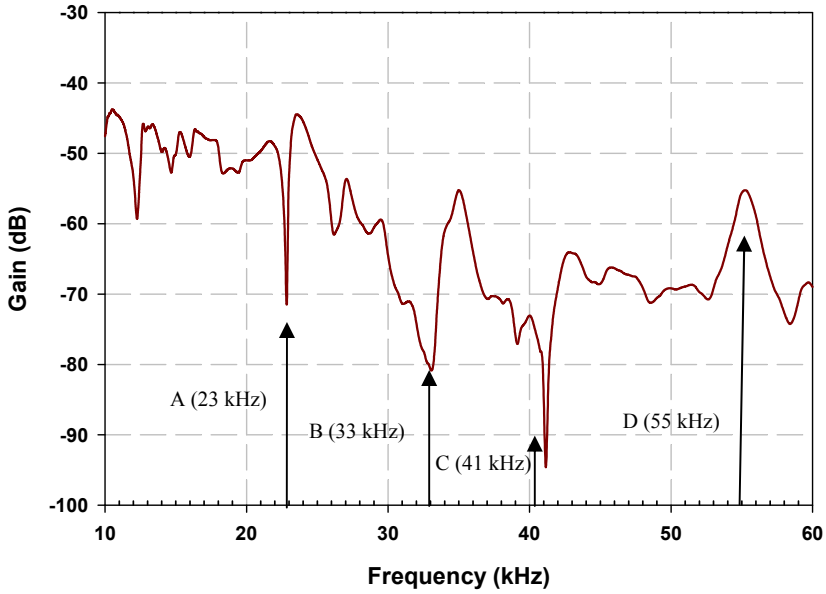

Figure 4-3: Calibration curve

4.4 Approach

Experimentation is a vital and integral part of engineering methods and plays an important role in product realization activities: new product design and formulation, and manufacturing process development. A well designed experiment is important because the results and conclusions that can be drawn depend to a large extent on the manner in which the data were recorded. In an experiment, typically one or more variables or factors are deliberately changed in order to observe the effect the changes have on one or more response variables. Experimental data are then used to derive an empirical model linking the outputs and inputs. These empirical models generally contain first and second-order terms. Screening designs are used to identify the few significant factors from a list of many

potential ones. In short, screening designs are economical experimental plans that focus on determining the relative significance of many main effects. This can be achieved using factorial designs (Montgomery 2005).

The correct approach to dealing with several factors is to conduct a factorial experiment. In this technique, factors are varied together instead of one at a time. By a factorial design, each complete trial or replication of the experiment for all possible combinations of the levels of the factors are investigated. The effect of a factor is defined to be the change in response produced by a change in the level of the factor. This is called a main effect as it refers to the primary factors of interest in the experiment. For some experiments, it is seen that the difference in response between the levels of one factor is not the same at all levels of the other factors. When this occurs, there is an interaction between the factors. As the number of factors in a 2^k factorial design increases, the number of runs required for a complete replicate of the design rapidly outgrows the resources of most experimenters. If the experimenter can reasonably assume that certain high-order interactions are negligible, information on the main effects and low-order interactions may be obtained by running only a fraction of the complete factorial experiment. Since we are able to choose fractions of a full design, the whole experimental research process is made more economical and efficient. These fractional factorial designs are among the most widely used types of designs for product and process design and for process improvement. One very important feature of this factorial experiment is factorials make efficient use of the experimental data.

The three basic principles of experimental design are randomization, replication, and blocking. Here for this study we have used replication in our design, as more number of samples of a kind can be tested for better accuracy. The ANOVA (Analysis of Variance) aids in determining the validity of the experimental design by testing the difference between two or more groups. When the F-value is larger than the significance F-value, the experiment design is considered to be valid, indicating that at least one of factors have an effect on the response variable. The F-value is computed from the mean square values, and Significance F-value is selected from the F-distribution tables based on the size of the sample, the number of factors, and the significance level selected which is 95% in this case. As the F-value is larger than the significance F-value, the linear model design is considered to be valid.

The ANOVA only shows that the experimental design as a whole is valid but all the factors considered in the design may not be relevant. The analysis following the ANOVA helps in determining the importance of all factors. The factors are analyzed on the basis of the corresponding p-value. The basic purpose of a factorial design is to economically investigate cause-and-effect relationships of significance in a given experimental setting. By a factorial design, each complete trial or replication of the experiment for all possible combinations of the levels of the factors are investigated. The effect of a factor is defined to be the change in response produced by a change in the level of the factor. This is called a main effect as it refers to the primary factors or interest in the experiment. For some experiments, it is seen that the difference in response between the levels of one factor is not the same at all levels of the other factors. When this occurs, there is an interaction

between the factors. The 2^k design is particularly useful in the early stages of experimental work, when many factors are likely to be investigated. It provides the smallest number of runs with which k factors can be studied factorial design; these designs are widely used in factor screening experiments as discussed later. As the number of factors in a 2^k factorial design increases, the number of runs required for a complete replicate of the design rapidly outgrows the resources of most experimenters. If the experimenter can reasonably assume that certain high-order interactions are negligible, information on the main effects and low-order interactions may be obtained by running only a fraction of the complete factorial experiment. Since we are able to choose fractions of a full design, the whole experimental research process is made more economical and efficient. These fractional factorial designs are among the most widely used types of designs for product and process design and for process improvement.

It is common to begin with several discrete or continuous input factors that can be controlled, that is, varied when desired by the experimenter and one or more measured output response variables which always are assumed to be continuous. In this particular case, a two level design is chosen due to the large number of factors involved. These levels "low" and "high" are denoted by "–" and "+" respectively and are chosen based on material availability and/or experience and are described in detail in Table 4-1.

Table 4-1: Factors distribution

Factors	**levels**	**Levels** ***Low (-)***	***High (+)***	***Units***	***Type***
thickness (*t*)	2	28	110	μm	continuous
weight (*w*)	2	20	50	g	continuous
area (*A*)	5	150, 196,225	270, 300	mm²	continuous
electrode (*e*)	2	Cu-Ni	Ag	n/a	discrete

A full factorial design, 2^4, with different levels and 2 replicates was considered. In the case of thickness, commercially available sizes dictated the low and high settings. PVDF polymer is available commercially coated with Silver and Copper-Nickel electrodes, so these values were set as high and low for our study. Applied weight was chosen up to 50 grams because the Bimorph was set as a cantilever beam for the experimental setup as shown in Figure 4-2, and addition of more weight could break the beam. For the factor, area, more levels were selected so as to see the behavior of the response variable with respect to area covered by the sensor. From the entries in Table 4-2 all factor effects such as main effects, first and second-order interaction effects can be calculated. The complete distribution is shown in Appendix A.

Table 4-2: Full factorial design with 4 factors at different levels

Pattern	t	w	A	e	Gain
−−11	-1	-1	1	L1	G_{--11}
−−11	-1	-1	1	L1	G_{--11}
−−11	-1	-1	1	L1	G_{--11}
−−12	-1	-1	1	L2	G_{--12}
−−12	-1	-1	1	L2	G_{--12}
−−12	-1	-1	1	L2	G_{--12}
−−21	-1	-1	2	L1	G_{--21}
−−21	-1	-1	2	L1	G_{--21}
−−21	-1	-1	2	L1	G_{--21}
−−22	-1	-1	2	L2	G_{--22}
⋮	⋮	⋮	⋮	⋮	⋮ ⋮
++52	1	1	5	L2	G_{++52}

A full factorial design with with 4 factors, β, γ, α, and τ can be represented by Equation 4-1. These variables represent the factors under study, y represents the response variable of gain, μ represent the average of all factors, and ε represents the error.

$$\begin{aligned} y_{ijklm} = {} & \mu + \tau_i + \beta_j + \gamma_k + \alpha_l \\ & + (\tau \cdot \beta)_{ij} + (\tau \cdot \gamma)_{ik} + (\tau \cdot \alpha)_{il} + (\beta \cdot \gamma)_{jk} + (\beta \cdot \alpha)_{jl} + (\gamma \cdot \alpha)_{kl} \\ & + (\tau \cdot \beta \cdot \gamma)_{ijk} + (\tau \cdot \beta \cdot \alpha)_{ijl} + (\beta \cdot \gamma \cdot \alpha)_{jkl} \\ & + (\tau \cdot \beta \cdot \gamma \cdot \alpha)_{ijkl} + \varepsilon_{ijklm} \end{aligned} \qquad \textbf{4-1}$$

5 Results and Discussion

This chapter discusses the results obtained from the Design of Experiments theory and the effects of the factors and their interactions. Prediction profiles, regression analysis, contour plots, and the analysis of variance are also discussed.

5.1 Design of Experiments

Once the materials, experimental setup, factors, and response variables are chosen, a design of experiments is carried out using statistical analysis tools and the software JMP 8.0. Through this technique a full factorial design can provide information on the factors effect if any, their relevance, and even develop a model to predict the performance of the developed sensor. A 95% confidence level is used for all the analysis and relevant factors are identified through *p-values* on the response variables. Conventionally for this analysis the 5% (less than 1 in 20 chance of being wrong) levels or the 95% confidence internal mark has be chosen such that the *p-value* has to be less than 0.05(Devore 2004).

5.2 Response Curve

Since the response variable used on the design of experiments is gain defined as the ratio of output signal to input signal, response quality may be poor. To ensure the signal obtained is of good quality, response curves are measured using an oscilloscope at specific frequencies. A response curve for a typical sensor is shown in Figure 5-1. This curve

shows that the sensor responds to the source with a delay of 0.7µsec and is not distorted in any way. Other frequencies were also checked but not included for clarity purposes.

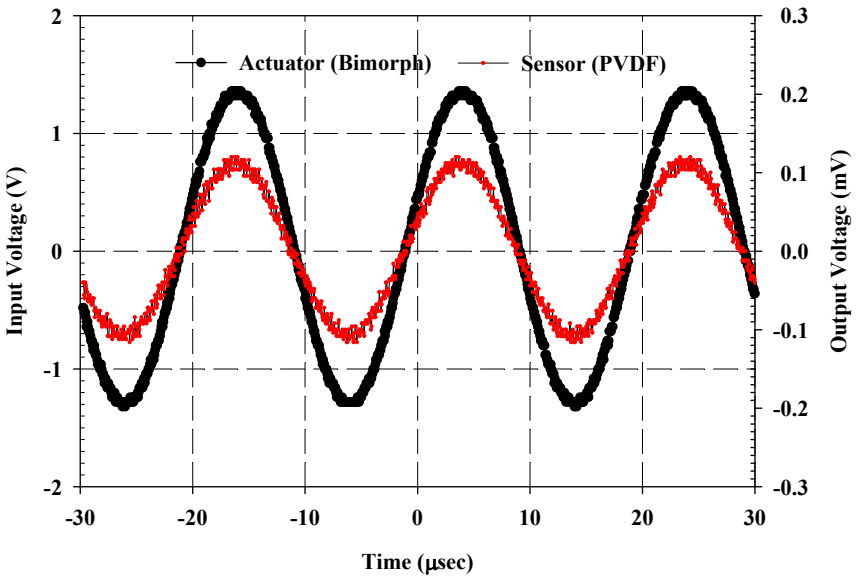

Figure 5-1: Typical sensor and actuator responses at 50 kHz with an input sinusoidal waveform of 1 Volt peak to peak magnitude and a sensor output of 0.23 volts

5.3 Gain Curve

Using the output of the sensor divided by the input to the actuator, a gain over a frequency range is obtained. Two approaches discussed in the experimental section setup were considered. The first one consisted on double sided tape. In this approach, the tape served a double purpose: as a coupling mechanism between the sensor and the skin, and as an adhesive to hold the sensor in place. Results using this technique however, were not reliable or repeatable and subject to large error. So as to reduce or minimize the error, a

second technique was utilized. Pressure, in the form of a counter weight is used to ensure good coupling between the sensor and the actuator. This technique provided more consistent and reliable results. A typical gain curve over the frequency is shown in Figure 5-2. These results show peaks in the ranges of 22 – 25 kHz and 52 – 55 kHz. These values are believed to be inherent to the Bimorph. The other peaks that can be seen with the accelerometer, but not the PVDF, may be due to the additional stresses the bimorph possesses due to the added weight of the accelerometer and are not considered for this study since PVDF does not add structural stresses to the beam. In addition all the samples show the same trend. All other tests are shown in Appendix A and omitted here for clarity purposes.

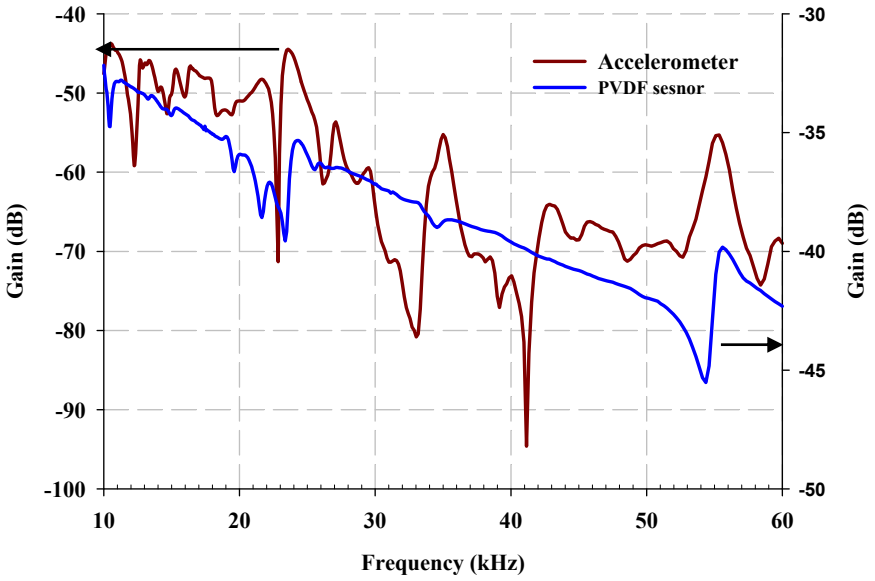

Figure 5-2: Typical gain vs. frequency response plot for a PVDF sensor with Cu-Ni electrodes, 28 microns thick and 150mm² surface area with a 50 grams counterweight

5.4 Statistical Analysis

Because of the pattern shown in Figure 5-2, a gain at 50 kHz was selected as a response variable to avoid errors in the area of the peaks. In this manner, statistical evaluation of all factors is possible and a model can be tested. An Analysis of Variance, ANOVA, is performed for the model shown in equation 4-1, and the results are summarized in Table 5-1. These results show that the model fitted to the data is statistically significant and the probability of the model not fitting the data is less than 0.0001.

Table 5-1: Analysis of Variance

Source	**Sum of Squares**	**Mean Square**	**F Ratio**
Model	2396.03	159.74	7.53
Error	2207.56	21.23	Prob > F
C. Total	4603.59		<.0001

These results indicate that a model exists for a specific combination of parameters shown in bold in Table 5.2: thickness, weight, area, and one electrode type are statistically significant. In particular, the interaction between weight, area, and thickness is quite significant as well as the interaction between thickness, area, and electrode. Higher order interactions were negligible, as well as the factors by themselves but are included in the model since that has an effect on the regression model overall.

The model developed is multi-dimensional as shown in Equation 4-1. In order to visualize the results, contour and three dimensional plots can be constructed. This is accomplished by leaving some of the parameters constant and varying 3 factors. Figure 5-3 shows the contour map of thickness and area as *x* and *y* variables, and the contour lines represent the gain. In this case, the electrodes are Copper Nickel electrodes with a constant weigth of 20 grams. This figure shows that samples with higher thickness had more response than the thinner samples, and area is almost constant.

Table 5-2: Regression Estimates

Term	***Estimate***	***p-value***
t	3.6083	<.0001*
t·w·A	-0.0243	0.0027*
w·A	-0.0197	0.0145*
t·A·e[cu]	0.0182	0.0236*
A·e[cu]	0.0175	0.0292*
w·e[cu]	0.8083	0.0573*
t·w·A·e[cu]	0.0150	0.0611
e[cu]	0.5583	0.1872
w·A·e[cu]	-0.0088	0.2711
t·w·e[cu]	0.4583	0.2783
A	0.0077	0.3372
w	0.2750	0.5146
t·A	0.0051	0.5250
t·w	0.2250	0.5938
t·e[cu]	-0.0250	0.9527

For instance in the case of Figure 5-3 an area of 250 mm^2 (red line) and a thickness of 70 μm (green line), a gain of is -40 dB is predicted. However, the same gain is attainable at an area of 230mm2 and the same thickness.

Similarly another contour plot is formed where the variables are weight and area as shown in Figure 5-4. In this case the electrode material is Cu-Ni and thickness of the sensor is kept constant at 45µm.

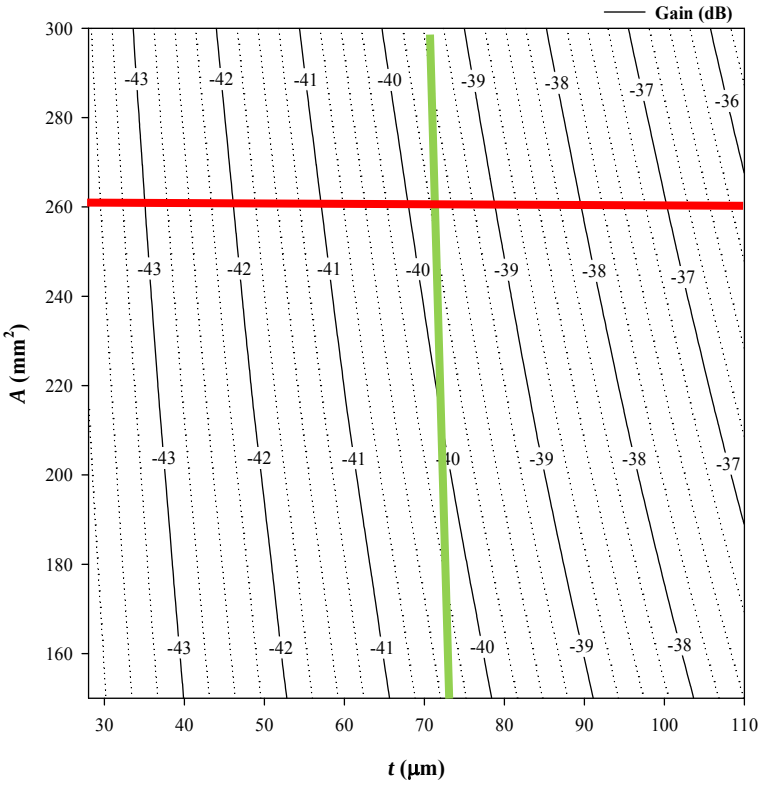

Figure 5-3: Contour plots for Gain at 50 kHz – weight 20 grams and Cu-Ni electrodes

From the Figure 5-4, it was observed that increase in weight when chosen carefully, does not alter the response signal for a particular constant area line. If the weight is kept constant and the area increases, the gain is slightly less. In short these two factors can be manipulated according to the desired location of the sensors.

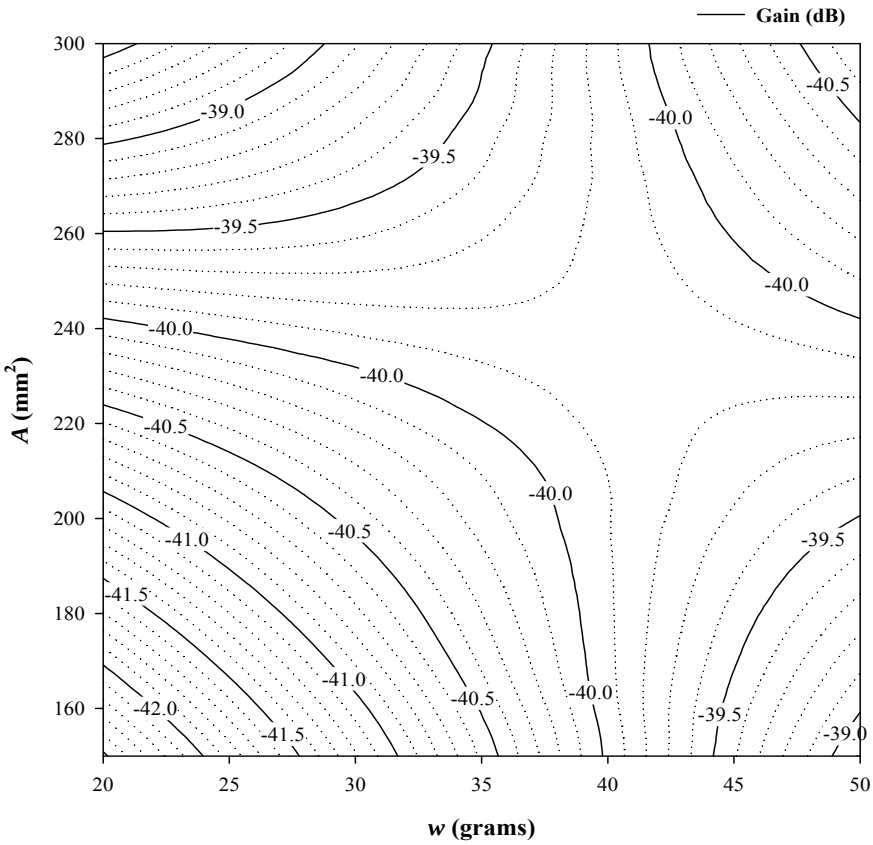

Figure 5-4: Contour plots for Gain at 50 kHz - 45µm thickness and Cu-Ni electrodes

To provide an overall picture of the relevance of each effect, Fig 5-5 is constructed. Though these graphs are constructed with only two points (max, and min) for each factor, slope of growth or decay can be easily spotted. For instance, among the factors tested, thickness had the most significant value on the design.

A more detailed view than contour plots and overall effects plots can be accomplished on three dimensions. Some variables are still kept constant as previously done with the contour plots.

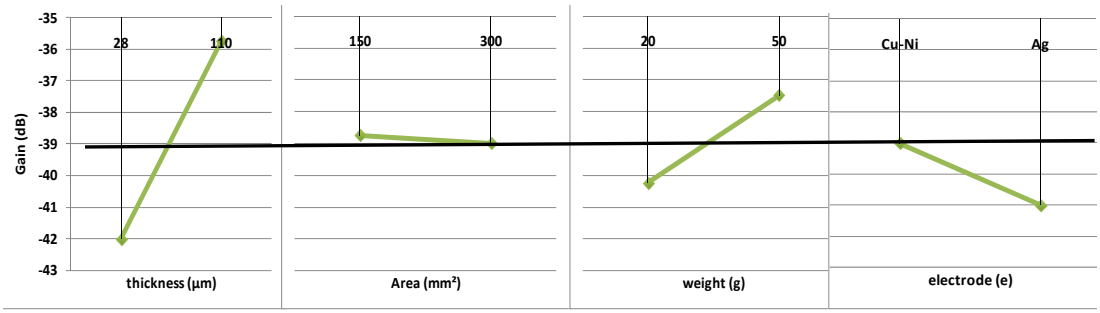

Figure 5-5: Main effects of each factor

Specifically, gain, area, and thickness are varied but electrode and weight are kept constant. Results are shown in Figure 5-6. In this case, a plane is easily visible and the optimized region is identified clearly: higher area and higher thickness increase gain linearly. This is not the case for Figure 5-7, where weight, area, and gain are shown at a constant thickness and electrode. In this case a complex plane with an inflexion area is shown. This shows that the weight (or applied pressure) is of utmost importance when optimizing gain.

To compare these results, numerical simulations were also carried out and details are shown in the next section.

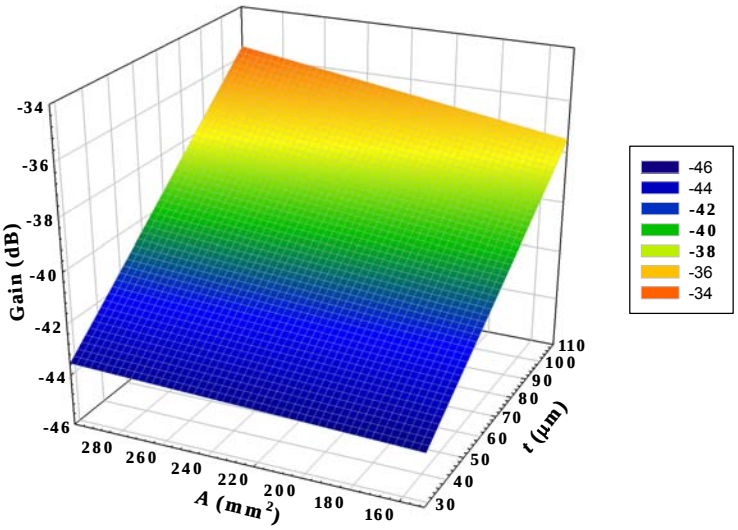

Figure 5-6: Gain at 50 kHz with a weight of 34 grams, Cu-Ni electrodes

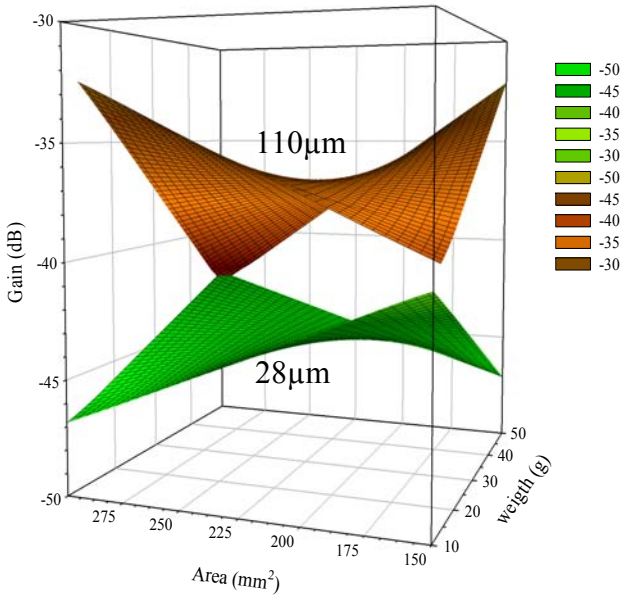

Figure 5-7: Gain at 50 kHz with Silver electrodes at two constant thickness values

6 Numerical Simulations

In order to investigate the physics behind the actuation and sensing mechanism, series of numerical modeling approach is required. In this chapter, effort has been made to model and simulate the performance of PZT-bimorph–PVDF setup. A design of experiments approach is performed to elucidate the effects of design factors and their relative importance in the physics. This chapter discusses the approach, modeling techniques and results of numerical modeling in conjunction to the experiments discussed in the earlier chapters.

6.1 Setup

The actuator, Bimorph, as discussed earlier (chapter 4) consists of PZT ceramic plates on either sides of the steel plate which, on application of external voltage, display the reverse piezoelectric effect. It is because of reverse piezoelectric effect, the bimorph undergoes a state of deformation in order to relieve the stresses induced by the application of voltage difference across its thickness. This deformation is thus transferred to the PVDF sensor which is mounted on the top of bimorph cantilever, thereby producing an electrical voltage difference across its thickness because of piezoelectric effect. The voltage generated by PVDF is proportional to the deformation it experiences. A distance of 5mm is marked as a reference point as shown in Figure 6-1, representing the top schematic view of the model. From one end actuator is held as a cantilever beam, its displacement at the edge

of the beam should be zero. For these simulations, Mylar was used for encasing material as shown in Figure 6–2; thickness of PVDF is varied in the study.

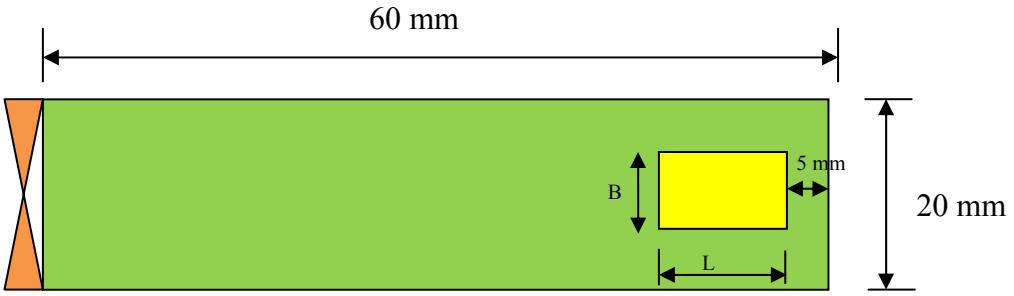

Figure 6-1: Schematic top view of the developed model

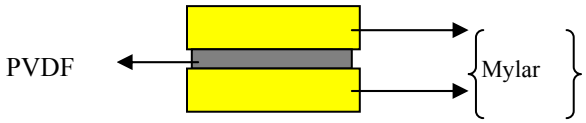

Figure 6-2: Schematic drawing of sensor

6.2 Mathematics of modeling

The complete model is simulated in ANSYS 11 which is capable of simulating this multiphysics problem. The bimorph and PVDF are modeled as 3-D anisotropic solid with the deflections and voltage as degrees of freedom. For linear piezoelectric materials, the linear constitutive equations relating the stress σ, strain ε, electric field E, are given by

$$\sigma_{ij} = C^{E}_{ijkl}\varepsilon_{kl} - e_{ijk}E_{k} \tag{6.1}$$

where ε_{kl} is the mechanical strain tensor, σ_{ij} is the mechanical stress tensor, E_k is the electric field vector, e_{ijk} is the piezoelectric constant tensor; C^{E}_{ijkl} is a 6 × 6, symmetric,

elastic stiffness constant tensor. In general, for anisotropic materials, there are 45 independent material constants: 21 elastic, 18 piezoelectric, and 6 dielectric properties. Fortunately, for the hexagonal class piezoelectric material polarized in the radial direction, some constants are zero due to crystal symmetry (Shiah and Huang 2006). Two commercial materials with distinct properties, PVDF and PZT-5A, are considered for sensing and actuation respectively. The material properties for PZT-5A, an active component of PZT-bimorph device are displayed in Table 6–1.

Table 6-1: Material constants of PZT 5A (Bhadauria et al 2009)

$C_{ijkl} \times 10^{10}$ (Pa)								
C_{1111}	C_{1122}	C_{1133}	C_{2222}	C_{2233}	C_{3333}	C_{1212}	C_{2323}	C_{1313}
12.03	7.52	7.51	12.03	7.51	11.1	2.11	2.11	2.26
Piezoelectric coefficients (C-m^{-2})					Permittivity (10^{-9} F-m^{-1})			Density (kg-m^{-3})
e_{15}	e_{14}	e_{31}	e_{32}	e_{33}	ε_{11}	ε_{22}	ε_{33}	7750
12.3	12.3	-5.35	-5.35	15.78	1730	1730	1700	

In contrast, PVDF has relatively low dielectric and piezoelectric constants compared to piezoelectric ceramics, for which it is widely used as a sensing device. The material properties are displayed in Table 6–2. As the actuator consists of a steel plate in between two PZT ceramics, its properties are also incorporated in the simulation. It has a density which is equal to 7800 kg/m^3 , Young Modulus E = 5.32 GPa, thickness equal to 0.01 mm and Poisson's ratio equal to 0.38. Mylar is used as the packaging material; it has a density which is equal to 1400 kg/m^3 , Youngs Modulus E = 5.32 GPa, Thickness equal to 0.005 inch and Poisson's ratio equal to 0.38. Also, a study is done to evaluate the performance of PVDF sensor by altering its size.

Table 6-2: Material properties of PVDF

$C_{ijkl} \times 10^{10}$ (Pa)								
C_{1111}	C_{1122}	C_{1133}	C_{2222}	C_{2233}	C_{3333}	C_{1212}	C_{2323}	C_{1313}
23.824	0.398	0.219	23.284	0.219	1.064	0.215	0.643	0.643
Piezoelectric coefficients ($C\text{-}m^{-2}$)					Permittivity (10^{-9} $F\text{-}m^{-1}$)			Density ($kg\text{-}m^{-3}$)
e_{15}	e_{14}	e_{31}	e_{32}	e_{33}	ε_{11}	ε_{22}	ε_{33}	1780
-0.135	-0.135	-0.13	-0.13	-0.276	1.1068	1.1068	1.0607	

6.3 Boundary Conditions

Bimorph, was set as a cantilever beam, its one end was fixed. Its displacement, due to the setup is zero. Pressure is applied as a coupling transmission medium on the sensor, the side view of the model is shown in Figure 6–3. As the study was to check the effect of factors on the response variable, applied pressure given was 20 and 50 grams. Input voltage given to the Bimorph was 1V, at a frequency of 50 kHz.

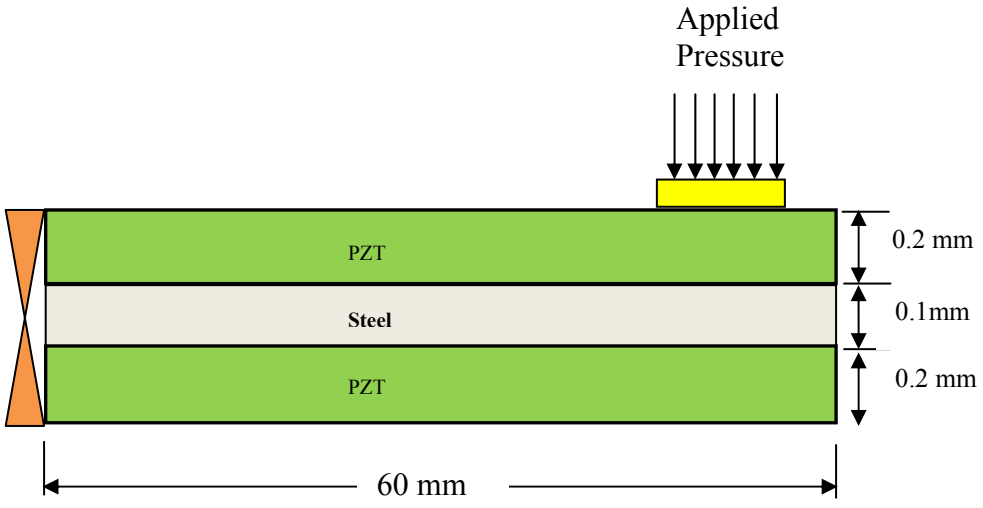

Figure 6-3: Schematic side view of the setup

Results from the experimental analysis showed that thicker PVDF polymer samples yielded better gain value, for the numerical approach also different thickness in order of 28 and 110 μm were also tested. The deflection of the bimorph was observed in z direction, and it was given a series type of connection across its geometry as seen in Figure 6-4.

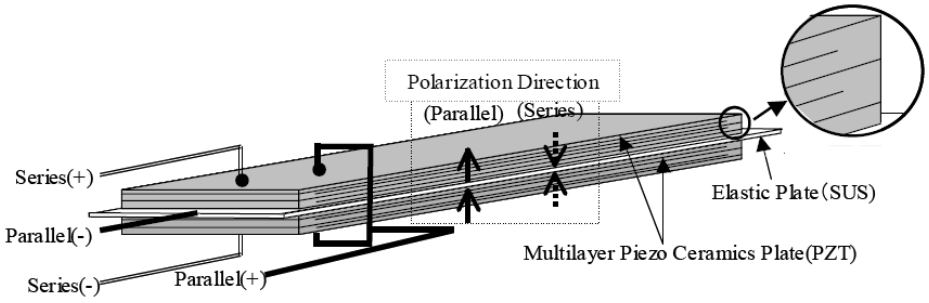

Figure 6-4: Bimorph connection-Parallel (Eriguchi et al. 2008)

Hexahedral elements with element size 0.0005 are used to mesh the geometry. The above mentioned value of element size is chosen after conducting a mesh independent study. There are 5 elements across thickness of PZT and Mylar while 3 elements are used across the steel and PVDF. For the piezoelectric materials SOLID5 elements are SOLID45 applied to model the problem whereas for the steel and packaging material. The swept frequency was 50 kHz.

6.4 Approach

A parametric study is carried out numerically to evaluate the performance characteristics with respect to actuating frequency of the PZT actuator. In this study, the response signal collected by the sensor has been investigated in detail by simulating the actuator and taking into account the complete physics of electro-mechanical coupling between the piezoelectric materials. Factors used in the design and development of the sensor for the testing part has been taken into consideration for the simulation. A factorial design 2^3 with factors area (*a*), thickness (*t*), applied weight (*w*), was developed. Electrode type and frequency are kept constant. Hence, the total number of designs is 8 as seen in Table 6-3.

Table 6-3: Design distribution (factors interactions)

Area (*a*)	**Thickness (*t*)**	**Applied weight (*w*)**
-1	-1	-1
+1	-1	-1
-1	+1	-1
+1	+1	-1
-1	-1	+1
+1	-1	+1
-1	+1	+1
+1	+1	+1

Table 6-4 represents the factor distribution and interactions, “+1” represents the “high” setting of a factor and “-1” represents the “low” setting of a factor.

Table 6-4: Factor distribution

Factor	**Low value (-1)**	**High value (+1)**
Thickness (*t)*	28 µm	110 µm
Area (*a*)	150 mm^2	300 mm^2
Applied Weight (*w*)	20 grams	50 grams

6.5 Results and Discussions

Each cycle was set at 100 intervals, and the results are taken out at t/T = 0.25, where t is the time and T is total time-period.and frequency f was set as 50 kHz. and compared for analysis, it was observed that the thicker samples yielded better output response (gain). Stress was also taken out across the PVDF thickness as shown in Table 6-5.

Table 6-5: Numerical results

Design	thickness	Area	Applied Weight	Gain (dB)		Stress
	(*t)* µm	(*a*) mm^2	(*w*) grams	Experimental	Numerical	mPa
1	28	150	20	-45	-157	251.6
2	28	300	20	-43	-159	283.9
3	28	150	50	-41	-158	248.9
4	28	300	50	-39	-160	287.4
5	110	150	20	-35	-138	240.2
6	110	300	20	-38	-137	238.9
7	110	150	50	-34	-134	238.4
8	110	300	50	-36	-135	223.6

As discussed above, Bimorph was fixed from one end, its deflection was measured maximum at the other free end. It showed a linear displacement as seen in Figure 6-5. The values are plotted in the negative direction of the z axis.

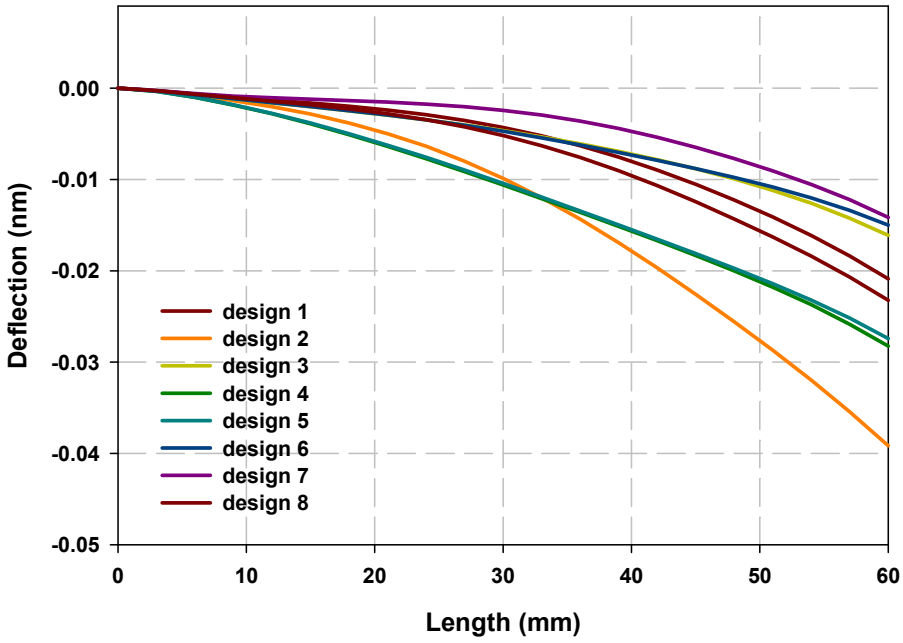

Figure 6-5: Bimorph tip deflection curve at 50 kHz, at 1Vpp applied sinusoidal waveform

Similarly, observing the effect of each factor on the response (gain), prediction profile of each factor are evaluated. Thickness did show a variation in the value of gain in accordance with its low and high value. Thicker samples had more optimized gain, similar trend was observed with the experimental analysis. Other factors like area and weight did

not have much steep slope as compared to thickness of PVDF polymer, as seen in Figure 6-6.

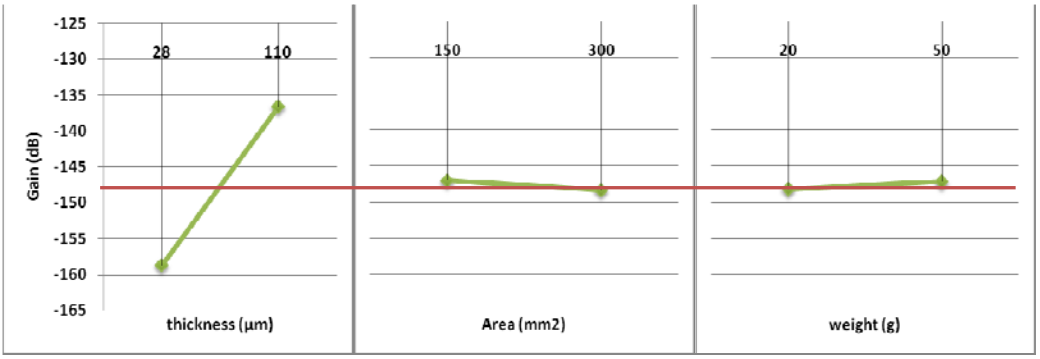

Figure 6-6: Main effect of factors - Numerical

The average gain value calculated for the developed design was -147 db, while the experimental average value was -39 db. Similar trends can be observed in the factors when comparing the results of numerical simulations and experimental analysis. Figure 6-7 shows the behavior of factors (Experimental) and their optimized values at low and high levels.

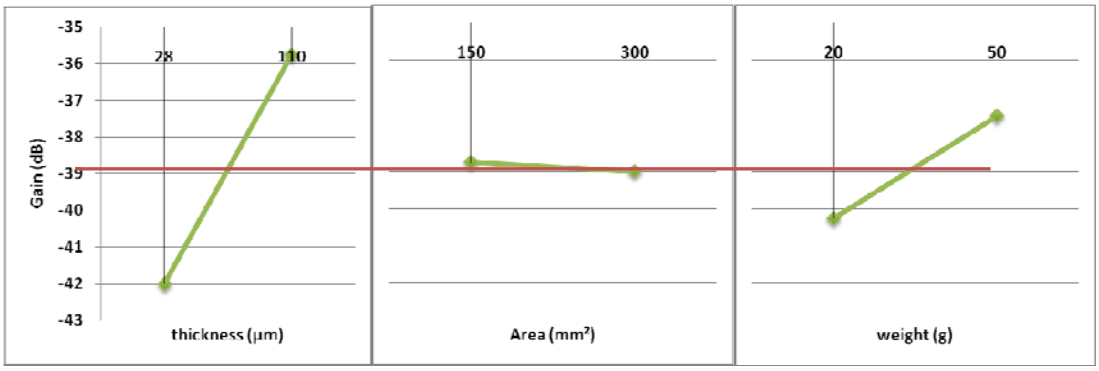

Figure 6-7: Main effect of factors -Experimental

Stress was measured across the PVDF polymer thickness, as seen in Table 6-5, samples with thickness 28 µm had more von misses stress as compared to 110 µm. Thickness had an inverse influence on the stress, when compared with the gain as seen in Figure 6-8.

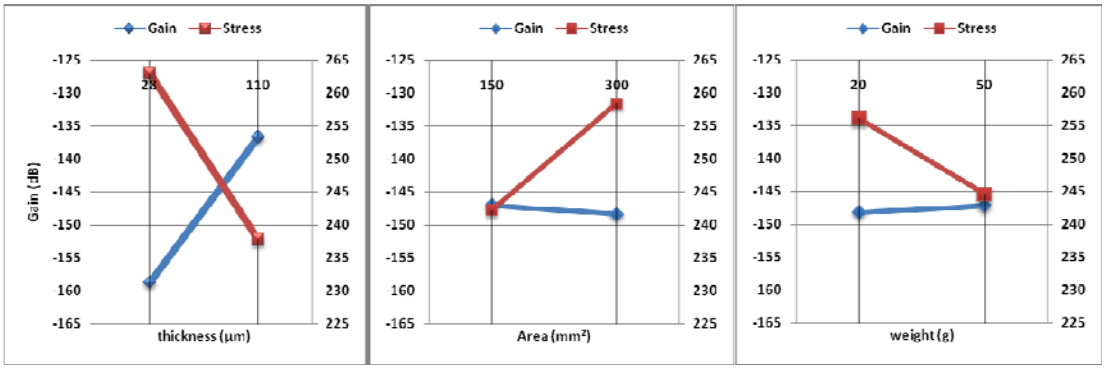

Figure 6-8: Stress and gain behavior observed

7 Design Prototypes

This chapter discusses the designs and prototypes developed for the sensors. Pressure mechanisms are developed. Initial testing and results of are also discussed.

7.1 Developed designs

The sensor developed has to fit over the closed human eyelid; the main design limitations are the dimensions of a human head and the eyelid. An initial design shown in Figure 7-1, shows the first generation ICP frames. These frames are used to provide a consistent application mechanism. In addition the design includes a mounting mechanism so that the sensor can be mounted on the glasses. Finally, to provide constant applied pressure, a tension band Scothmate™ 3M, Hook and Loop fastening system is incorporated.

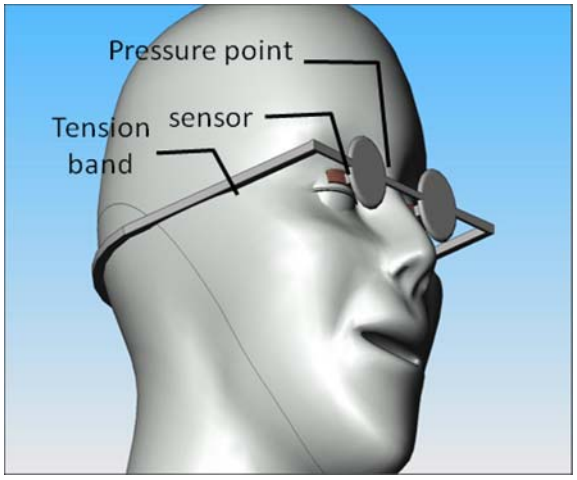

Figure 7-1: Sample prototype view, ICP- I

However, the prototype shown in Figure 7-1 does not include adjustments for different head sizes and eye positioning. Another prototype is then developed as shown in Figure 7-2. This design was built using a Stratasys FDM 3000™ Rapid prototyping Machine (FDM-3000).

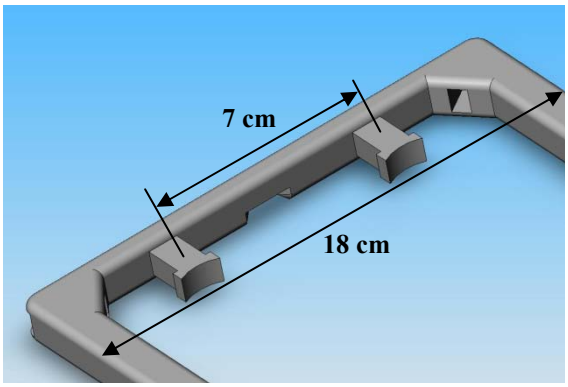

Figure 7-2: Initial frame design, ICP- II

To accommodate to the curved nature of the eye, holders are fabricated with a radius of curvature as shown in Figure 7-3.

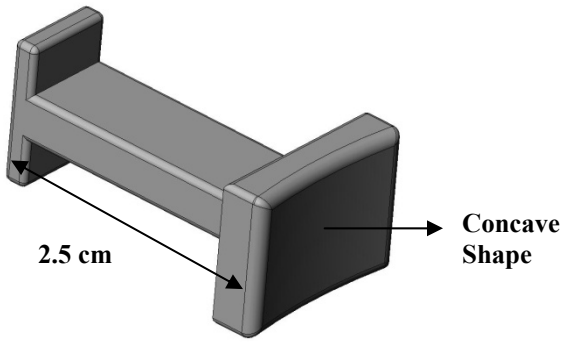

Figure 7-3: Holder

The final design, shown in Figure 7-4, accommodates for different head and bridge (distance between the eyes) dimensions. New frames were designed and developed so that they had the sliding mechanism for the holders, and are overall lighter.. Figure 7-4 shows a view of the adjustable sliding frames, ICP-III.

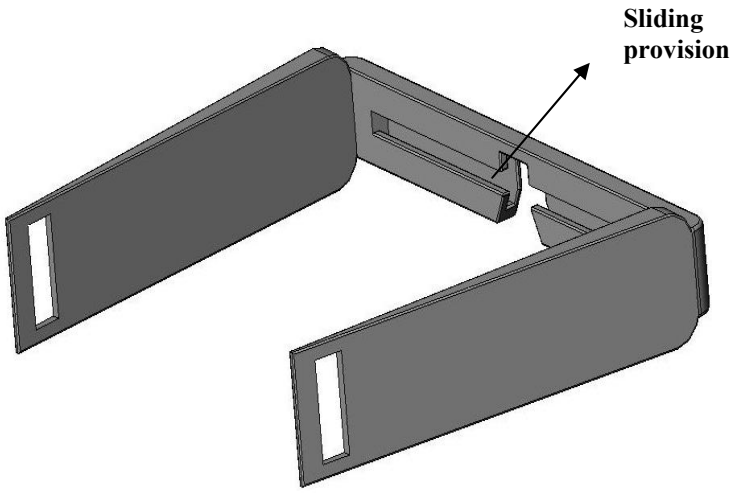

Figure 7-4 : Modified frames, ICP-III

7.2 Prototype Design Testing

Once the modified frames were designed, the next step was to mount the sensor. Frames were made using Stratasys FDM 3000™ Rapid prototyping Machine (FDM-3000). The material used was Acrylonitrile Butadiene Styrene (ABS). The final prototype weight is approximately 65 grams, addressing one of the major concerns. Reliability and

repeatability of the recorded signals through these frames and sensors combinations is also tested. Testing includes mounting different sensors and verifying the quality of the signal.

7.2.1 Repeatability

The main idea here was to check the nature of the signal of the same sensor on a human subject at different set times. An HP 35670A Dynamic Signal Analyzer was used to take the Fast Fourier Transform (FFT) of the received signal. Tests were performed every 10 minutes. Figure 7 (a) shows the results of the tests performed across frequency range of 20-60 kHz and Figure 7(b) shows an enhanced view of the output signal from 20- 30 kHz. Test1 and Test 2 performed 10 minutes apart in the same subject and using the same frame-sensor combination shows that the obtained signal is repeatable.

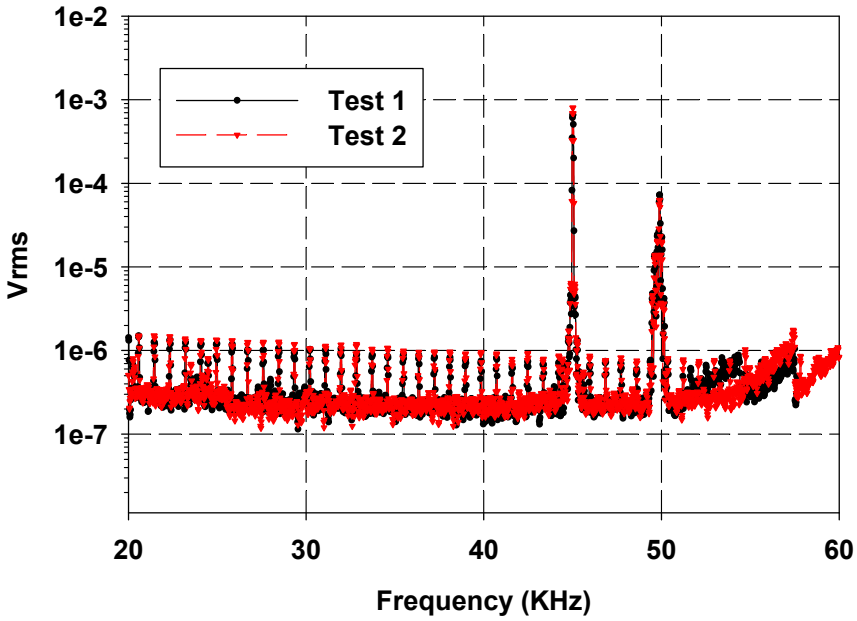

Figure 7-5: Output signal of sensor- repeatability test

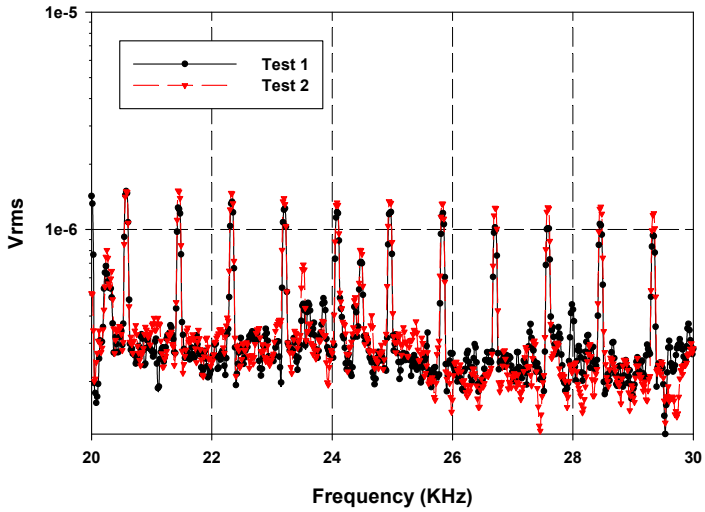

Figure 7-6: Output signal from 20-30 kHz

7.2.2 Reliability

In this phase, different sensors are placed on the frames and tested on the same subject. Figure 7-6 shows the output signal measured when using two different sensors that are manufactured, and assembled in the laboratory. This figure again shows that the results are quite reliable and the mounting and manufacturing of the devices is sound and consistent.

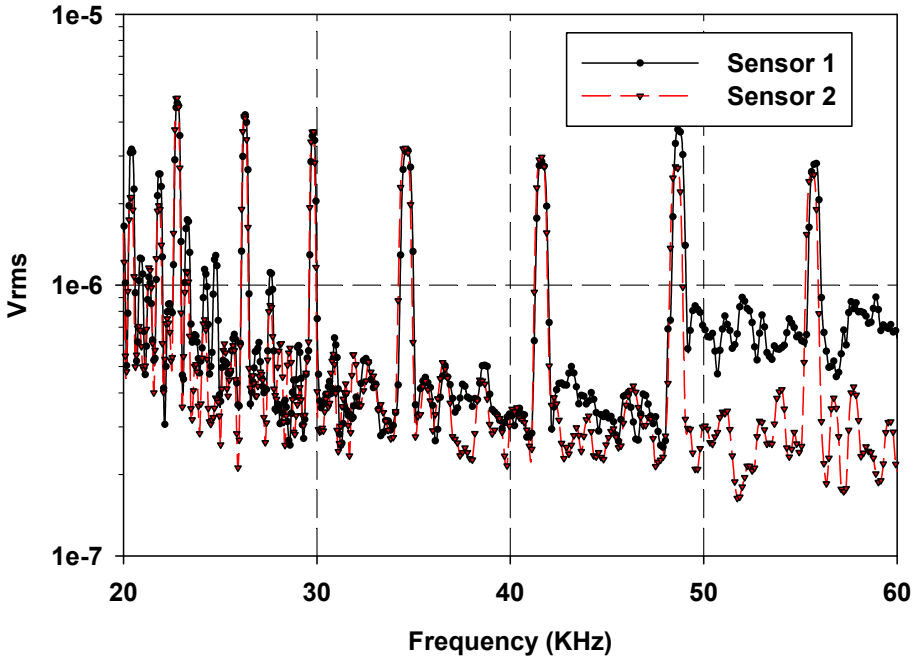

Figure 7-7: Output signal-reliability test

7.2.3 Sensitivity

To characterize the behavior of the sensor with respect to the applied voltage to the actuator, a sensitivity test is performed. By applying voltage ranging from 0.1 to 1V to the actuator-sensor setup described in section 4.2, the response of the sensor can be documented and measured. For these tests a constant weight of 20 grams was used and the tested frequency was 50 kHz. Results are shown in Figure 7-8. It was observed the output measured by the sensor was linearly proportional to the applied voltage to the actuator. The sensitivity was measured to be 0.2111mV/V.

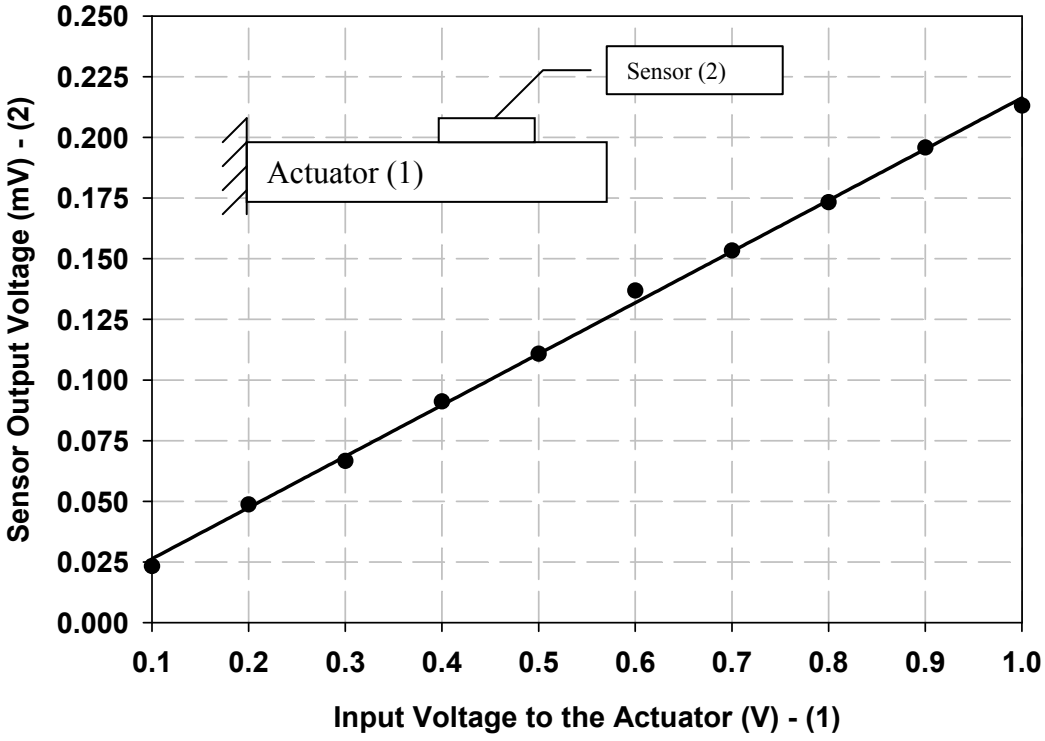

Figure 7-8: Measured Output Voltage at 50 kHz

8 Conclusions

A PVDF sensor to monitor ICP is developed and optimized using a design of experiments approach along with numerical simulations. The sensor is designed to operate in the frequency range of 20-60 kHz, without any additional power supplied or signal filtering or amplification scheme. In addition, the sensor is incorporated into a frame that provides reliable and repeatable results. The sensors were constructed from three main components: the piezoelectric sample itself, electrical leads that conduct the signal, and a packaging layer. To ensure the proper packaging of the sensor material different encasing materials were tested. It was observed that High Performance Scotch material (3M) had the highest peeling force of all the materials tested.

To optimize the sensor response and narrow down the variables that have a significant effect on the sensor performance, an experiment is designed to simulate the signal type that the sensor is supposed to be monitoring. This in itself is not a trivial matter since the vibration source has to perform in the frequency range of 20-60 kHz. Most magnetic commercially available shakers cannot perform in this frequency ranges without large power supplies. So in order to overcome these difficulties, a Bimorph was used as a source of vibration for the study. This device had parallel polarization direction and operated with a 1Volt-sinusoidal input waveform. An Accelerometer was used to calibrate the Bimorph which had a sensitivity of 10mV/g. Results indicated that the average vibration levels were in the order of 0.1g.

Another challenge of developing an experimental setup was sensor placement and adhesion. Several approaches, including double sided tape were attempted. Double sided tape and other adhesives utilized to maintain the PVDF sensor to the Bimorph failed by providing inconsistent and unrepeatable results. To minimize error, pressure, in the form of a counter weight was used to ensure good coupling between the sensor and the actuator. This technique provided more consistent and reliable results.

Once the experimental setup was designed, four factors were tested: sensor thickness, sensor area, sensor electrodes, and the applied counterweight. The complete set of experiments consisted of a 2^4 full factorial design at different levels and two replications.

Using the design developed, the results show that the main contributor to the gain is sensor thickness. Other factors in combination with each other also had an effect on the design and the response value, gain.

Numerical simulations were performed to model and simulate the performance of PZT-bimorph–PVDF setup. A 2^3 full factorial design was developed, using thickness, counterweight, and area as factors with gain as response variable. Results are compared with experimental results. The simulations showed that thicker samples yielded better gain of approximately -130 dB. Though these values were smaller than the experimental results, trends remain similar. That is, thickness is the most significant factor if gain is to be maximized. Differences can be observed on applied pressure effects on gain. Frames were developed for use on the head and eyes. These frames provided the sensor with tension to

hold in place. They were made using Stratasys FDM 3000™ Rapid prototyping Machine (FDM-3000).

To characterize the sensitivity of the sensor a calibration curve was performed. The calibration curve was measured using the same experimental setup used for all tests with the exception of the applied voltage. In this case the applied voltage to the actuator was varied from 0.1 to 1Volt, with a constant pressure (weight = 20grms) and a constant frequency 50kHz. It was observed the output measured by the sensor was linearly proportional to the applied voltage to the actuator. The sensitivity was measured to be 0.211mV/V. The final prototype of the ICP glasses weighted approximately 65 grams and had sliding mechanism for the holder, addressing one of the major concerns: adjustment for each patient and to provide consistent and reliable measurements.

9 Future Work

Developing the sensor and a setup to provide reliable measurements is only the first part to non-invasively monitor ICP. Another critical component of the technique is the actuator that will actuate a human skull. The actuator has to be a low voltage device that provides a high enough amplitude signal to be transmitted through the brain Cerebrospinal fluid. Next steps of the study would include incorporation of an actuator in the design. As simulation of head is one of the concerns, developing an actuator which would be portable, biocompatible, less expensive and light weight. One of the issues related to the actuator can be its level of actuation, how much input signal can be given to it. Once the actuator is developed, then testing of the sensor can be done while simulating the brain simultaneously.

This involves simulation of the medium, developing an appropriate setup and obtaining the appropriate IRB approvals. Finally, the whole setup needs to be tested and compared to traditional techniques.

References

Lundberg, N., Troupp, H., and Lorin, H., "Continuous recording of ventricular fluid pressure in patients with severe acute traumatic brain injury (Class II)," J Neurosurg, 75, pp. 581–590, 1965.

Robertson, C. S., Valadka, A. B., Hannay, H. J., Contant, C. F., Gopinath, S. P., Cormio, M., Uzura, M., Grossman, R. G., "Prevention of secondary ischemic insults after severe head injury," Crit Care Med, **27**, pp. 2086–95, 1999.

Mayhall, C. G., Archer, N. H., Lamb, V. A., Spadora, A. C., Baggett, J. W., Ward, J. D., Narayan, R. K., "Ventriculostomy-related infections. A prospective epidemiologic study," N Engl J Med, 310(3), pp. 553–9, 1984.

Park, E., Bell, J. D., Baker, A. J., "Traumatic brain injury: Can the consequences be stopped?," Canadian Medical Association Journal, 178(9), pp. 1163–70, 2008.

Xiong, Y., Lee, C. P., and Peterson, P. L., "Mitochondrial dysfunction following traumatic brain injury." In Head Trauma: Basic, Preclinical, and Clinical Directions, 25, pp. 257-280, 2001.

Smith**,** M., "Monitoring Intracranial Pressure in Traumatic Brain Injury," Anesth Analog, 106, pp. 240-248, 2008.

Bader, M. K., Littlejohns, J., Palmer, S., "Ventriculostomy and intracranial pressure monitoring: in search of a 0% infection rate," Heart Lung, 24(2), pp. 166–172, 1995.

Czosnyka, M., Pickard, J., "Monitoring and interpretation of intracranial pressure," Journal of Neurology, Neurosurgery, and Psyciatry, **7**5, pp. 813-821, 2004.

Kocan, M., "Ask The Experts," Critical Care Nurse, 22, pp. 70-73, 2002.

Munch, E., Weigel, R., Schmiedek, P., Schurer, L.," The Comino intracranial pressure device in clinical practice: reliability, handling characteristics and complications," Acta Neurochir 140, pp. 1113–1119, 1998.

Citerio, G., Andrews, P. J., "Intracranial pressure Part two: clinical applications and technology," Intensive Care Med, 30, pp. 1882–5, 2004.

Buki, B., Chomicki, A., Dordain, M., Lemaire, J. J., Chazal, J., Avan, P., Wit, H., "Middle-ear Influence on Otoacoustic Emissions. II: Contributions of Posture and

Intracranial Pressure," Hearing Research, 140, pp. 202-211, 2000.

Bekesy, V. G., "Vibration of the head in a sound field and its role in hearing by bone conduction," J Acoust Soc Am, 20, pp. 749-760, 1948.

Lashutka, M., Chandra, A., Murray, H., Phillips, G., Hiestand, B., "The relationship between introcular pressure to intracranial pressure," Ann Emerg Med, 43, pp.585-591, 2004.

C. Suplee, Is the Sky the Limit in the Future? The Virginian-Pilot, Business News, Wednesday, January 8, 1997, p. D-1.

Huang, J.H. and Kuo, W.S. ''Micromechanics Determination of the Effective Properties of Piezoelectric Composites Containing Spatially Oriented Shorted Fibers,'' Acta Metallurgica, 44(12): 4889–4898, 1996.

Sheeran, P., Bland, J. M., Hall, G. M., "Intraocular pressure changes and alteration in intracranial pressure", Lancet, pp. 255:889, 2000.

United States patent # 20070123796.

Fledelius, H. C., "Pre-term delivery and the growth of the eye: An oculometric study of eye size around term-time," Acta Ophthalmologica (Suppl.), 204, pp. 10-15, 1992.

Denis, D., Righini, M., Scheiner, C., Volot, F., Boubli, L., Dezard, X., "Ocular growth in the fetus. 1. Comparative study of axial length and biometric parameters in the fetus," Ophthalmologica, 207(3), pp. 117-124, 1993.

Insler, M. S., Cooper, H. D., May, S. E., Donzis, P. B., "Analysis of corneal thickness and corneal curvature in infants," CLAO Journal, 13(3), pp. 182-184, 1987.

Larsen, J. S., "The sagittal growth of the eye. IV. Ultrasonic measurement of the axial length of the eye from birth to puberty," Acta Ophthalmologica (Copenh), 49(6), pp. 873-886, 1971.

http://www.meas-spec.com/piezo-film-sensors.aspx

http://wiretron.com/

Dogan, A., Tressler, J., and Newnham, R.E., "Solid-State Ceramic Actuator Designs," AIAA, Vol. 39, No. 7, 2001.

http://www.jmp.com/, MP User Guide, Release 8 Copyright © 2008, SAS Institute., Cary, NC, USA. ISBN 978-1-59994-924-6.

Devore, J. L., "Probability and Statistics for Engineering and the Sciences," Duxbury Thomson Learning, 2004.

Finkelstein , E. A., Corso, P. S., Miller, T. R., Incidence and Economic Burden of Injuries in the United States. New York (NY): Oxford University Press; 2006.

Czosnyka, M., Association between arterial and intracranial pressures. Br J Neurosurg;14:127–8, 2000.

B. Jaffe, W.R. Cook, H. Jaffe, Piezoelectric Ceramics, Academic Press, New York, 1971

Langlois, J. A., Rutland-Brown, W., Thomas, K. E., Traumatic Brain Injury in the United States: Emergency Department Visits, Hospitalizations, and Deaths. Atlanta (GA): Centers for Disease Control and Prevention; 2004.

Thurman, D., Alverson, C., Dunn, K., Guerrero, J., Sniezek, J.," Traumatic brain injury in the United States: a public health perspective", Journal of Head Trauma and Rehabilitation, 14(6), pp. 602–615, 1999.

Hargens A. R., "Fluid shifts in vascular and extravascular compartments", Journal of Applied Physiol, 54, pp. 1003-1009, 1983.

Thornton W. E., "Anthropometric changes and fluid shifts", ln:NASA SP-377, pp 330-338, 1977.

Marshall, L. F., Gautille, T, Klauber, M. R, "The outcome of severe closed head injury", J Neurosurg, **75:** S28–36, 1991.

Graham, D. I., Ford, I., Adams, J. H., "Ischaemic brain damage is still common in fatal non missile head injury," J Neurol Neurosurg Psychiatry, 52, pp. 346–50, 1989.

DeWitt, D. S., Jenkins, L. W., Prough, D. S., " Enhanced vulnerability to secondary ischemic insults after experimental traumatic brain injury," New Horizons; 3**:** 376–83, 1995.

Ostrup, R. C., Luerssen, T. G., Marshall, L. F., "Continuousmonitoring of intracranial pressure with a miniaturized beroptic device," J Neurosurg, 67, pp. 206–209, 1987.

Piek, J., Kosub, B., Kuch, F., “A practical technique for continuous monitoring of cerebral tissure pressure in neurosurgical patients Preliminary results,” Acta Neurochir (Wien), 87, pp. 144–149, 1987.

.

Piek, J., Bock, W. J., “ Continuousmonitoring of cerebral tissue pressure in neurosurgical practice Experiences with 100 patients,” Intensive Care Med, 16, 184–188, 1990.

Czech, T., Korn, A., Reinprecht, A., “Clinical evaluation of a new epidural pressure monitor,” Acta Neurochir (Wien), 125, pp. 169–172, 1993.

Yau, Y. H., Piper, I. R., Clutton, R. E., Whittle, I. R., “Experimental evaluation of the Spiegelberg intracranial pressure and intracranial compliance monitor Technical note,” J Neurosurg, 93, pp. 1072–1077, 2003.

Barlow, P., Mendelow, A. D., Lawrence, A. E., “Clinical evaluation of two methods of subdural pressure monitoring,” J Neurosurg, 63,pp. 578-582, 1985.

Chambers, I. R., Kane, P. J., Choksey, M. S., “An evaluation of the Camino ventricular bolt system in clinical practice,” Neurosurgery, 33, pp. 866-868, 1993.

Chambers, I. R., Mendelow, A. D., Sinar, E. J., “A clinical evaluation of the Camino subdural screw and ventricular monitoring kits,” Neurosurgery, 26, pp. 421-423, 1990.

Gambardella, G., d'Avella, D., Tomasello, F., “Monitoring of brain tissue pressure with a fiberoptic device,” Neurosurgery, 31, pp. 918-921, 1992.

Gambardella, G., Zaccone, D., Cardia, E., “Intracranial pressure monitoring in children: Comparison of external ventricular device with the fiberoptic system,” Childs Nerv Syst, 9, pp. 470-473, 1993.

Gopinath, S. P., Robertson, C. S., “Clinical evaluation of a miniature strain-gauge transducer for monitoring intracranial pressure,” Neurosurgery, 36, pp. 1137-1141, 1995.

Schickner, D. J., Young, R. F., “Intracranial pressure monitoring: Fiberoptic monitor compared with the ventricular catheter,” Surg Neural, 7, pp. 251-254, 1992.

Schwarz, N., Matuschka, H., Meznik, A., “The Spiegelberg device for epidural registration of the ICP,” Unfallchirurgie, 95, pp. 113-117, 1992.

Yablon, J. S., Lantner, H. J., McCormack, T. M., “Clinical experience with a fiberoptic intracranial pressure monitor,” J Clin Monit 9:171-175, 1993.

Wersing, W., Schnoller, and Wahl, H., "Monolythic multilayer piezoelectric ceramics," Ferroelectrics, Vol. 68, pp.145-146, 1986.

Weaver, D. D., Winn, H. R., Jane, J. A., "Differential intracranial pressure in patients with unilateral mass lesions," J Neurosurg, 56, pp. 660-665, 1982.

Jospehson, L., "Management of increased intracranial pressure: A primer for the non-neuro critical care nurses," Dimensions Critical Care Nursing, 23(5), pp. 194-207, 2004.

Arbour, R., "Intracranial Hypertension Monitoring and Nursing Assessment," Critical Care Nurse, 24, pp. 19-32, 2004.

Gray, W. P., Palmer, J. D., Gill, J., "A clinical study of parenchymal and subdural minature strain-gauge transducer for monitoring intracranial pressure," Neurosurgery, 39, pp. 927–931, 1996.

Vassilyadi, M., Ventureyra, E. C., "Neuroendoscopic intracranial pressure monitoring," Child Nerv Syst, 18, pp. 147–148, 2002.

Bray, R. S., Chodroff, N. G., Narayan, R.K., "A new beroptic monitoringdevice: Development of the ventricularbolt," Intracranial Pressure VII, New York: Springer-Verlag, pp. 45–47, 1989.

Poca, M. A., Sahuquillo, J., Arribas, M., Baguena M., Amoros, S., Rubio, E., " Fiberoptic intraparenchymal brain pressure monitoring with the Camino V420 monitor: Reflections on our experience in 163 severely head-injured patients," J Neurotrauma, 19, pp. 439–448, 2002.

Chapman, P. H., Cosman, E. R., Arnold, M. A., "The relationship between ventricular fluid pressure and body position in normal subjects and subjects with shunt: A telemetric study," Neurosurgery, 36, pp. 181–189, 1990.

Holloway, K. L., Bames, T., Choi, S., "Ventriculostomy infections: The effect of monitoring duration and catheter exchange in 584 patients," J Neurosurg, 85, pp. 419-424, 1996.

Luerssen, T. G., Chesnut, R. M., van Berkum, Clark, M., "Post traumatic cerebrospinal fluid infections in the Traumatic Coma Data Bank: The influence of the type and management of monitoring," Intracranial Pressure VIII, Berlin, Springer-Verlag, pp. 42-45, 1991.

Barlow, P., Mendelow, A. D., Lawrence, A. E., “Clinical evaluation of two methods of subdural pressure monitoring,” J Neurosurg, 63, pp. 578-582. 1985.

North B., Reilly P., “Comparison among three methods of intracranial pressure recording,” Neurosurgery, 18, pp. 730, 1986.

Bratton, S. L., Chestnut, R. M., Ghajar, J., Harris, O., “Intracranial Pressure Mointoring Technology,” Journal of Neurotauma, Vol 24, pp. S45-54, 2007.

Larsen, J. S., , “The sagittal growth of the eye. IV. Ultrasonic measurement of the axial length of the eye from birth to puberty,” Acta Ophthalmologica (Copenh), *49*(6), pp. 873-886, 1971.

"The effect of elevated Intra cranial pressure on the vibrational response of the bovine head", Annals of Biomedical Engineering, vol. 23, pp. 720-727, 1995.

"A noninvasive approach to Intra cranial pressure monitoring", Journal of Clinical Engineering, vol. 7, pp. 73-78, 1982.

Singer, E., “Brain Trauma in Iraq,” Technology Review, April/May, 2008.

Bendo, A. A., Kass, I. S., Hartung, J., Cottrell, J. E., "Anesthesia for Neurosurgery, Chapter 28, in: Clinical Anesthesia”, 4th ed, Barash, PG, Cullen, BF, Stoelting, RK (eds) pp 777-789, Philadelphia, PA., Lippincott Williams & Wilkins, 2001.

Mokri, B., "The Monro-Kellie hypothesis: applications in CSF volume depletion", Neurology **56** (12), pp. 1746–8, 2001.

Appendix A: Factor Distribution

Pattern	t	w	A	e	Gain
−−11	-1	-1	1	L1	G_{--11}
−−11	-1	-1	1	L1	G_{--11}
−−11	-1	-1	1	L1	G_{--11}
−−12	-1	-1	1	L2	G_{--12}
−−12	-1	-1	1	L2	G_{--12}
−−12	-1	-1	1	L2	G_{--12}
−−21	-1	-1	2	L1	G_{--21}
−−21	-1	-1	2	L1	G_{--21}
−−21	-1	-1	2	L1	G_{--21}
−−22	-1	-1	2	L2	G_{--22}
−−22	-1	-1	2	L2	G_{--22}
−−22	-1	-1	2	L2	G_{--22}
−−31	-1	-1	3	L1	G_{--31}
−−31	-1	-1	3	L1	G_{--31}
−−31	-1	-1	3	L1	G_{--31}
−−32	-1	-1	3	L2	G_{--32}
−−32	-1	-1	3	L2	G_{--32}
−−32	-1	-1	3	L2	G_{--32}
−−41	-1	-1	4	L1	G_{--41}
−−41	-1	-1	4	L1	G_{--41}
−−41	-1	-1	4	L1	G_{--41}
−−42	-1	-1	4	L2	G_{--42}
−−42	-1	-1	4	L2	G_{--42}
−−42	-1	-1	4	L2	G_{--42}
−−51	-1	-1	5	L1	G_{--51}
−−51	-1	-1	5	L1	G_{--51}
−−51	-1	-1	5	L1	G_{--51}
−−52	-1	-1	5	L2	G_{--52}
−−52	-1	-1	5	L2	G_{--52}
−−52	-1	-1	5	L2	G_{--52}
−+11	-1	1	1	L1	G_{-+11}
−+11	-1	1	1	L1	G_{-+11}
−+11	-1	1	1	L1	G_{-+11}
−+12	-1	1	1	L2	G_{-+12}
−+12	-1	1	1	L2	G_{-+12}
−+12	-1	1	1	L2	G_{-+12}
−+21	-1	1	2	L1	G_{-+21}
−+21	-1	1	2	L1	G_{-+21}
−+21	-1	1	2	L1	G_{-+21}
−+22	-1	1	2	L2	G_{-+22}
−+22	-1	1	2	L2	G_{-+22}
−+22	-1	1	2	L2	G_{-+22}
−+31	-1	1	3	L1	G_{-+31}
−+31	-1	1	3	L1	G_{-+31}
−+31	-1	1	3	L1	G_{-+31}
−+32	-1	1	3	L2	G_{-+32}
−+32	-1	1	3	L2	G_{-+32}
−+32	-1	1	3	L2	G_{-+32}
−+41	-1	1	4	L1	G_{-+41}
−+41	-1	1	4	L1	G_{-+41}
−+41	-1	1	4	L1	G_{-+41}
−+42	-1	1	4	L2	G_{-+42}
−+42	-1	1	4	L2	G_{-+42}
−+42	-1	1	4	L2	G_{-+42}
−+51	-1	1	5	L1	G_{-+51}
−+51	-1	1	5	L1	G_{-+51}
−+51	-1	1	5	L1	G_{-+51}
−+52	-1	1	5	L2	G_{-+52}
−+52	-1	1	5	L2	G_{-+52}
−+52	-1	1	5	L2	G_{-+52}

Pattern	t	w	A	e	Gain
+−11	1	-1	1	L1	G_{+-11}
+−11	1	-1	1	L1	G_{+-11}
+−11	1	-1	1	L1	G_{+-11}
+−12	1	-1	1	L2	G_{+-12}
+−12	1	-1	1	L2	G_{+-12}
+−12	1	-1	1	L2	G_{+-12}
+−21	1	-1	2	L1	G_{+-21}
+−21	1	-1	2	L1	G_{+-21}
+−21	1	-1	2	L1	G_{+-21}
+−22	1	-1	2	L2	G_{+-22}
+−22	1	-1	2	L2	G_{+-22}
+−22	1	-1	2	L2	G_{+-22}
+−31	1	-1	3	L1	G_{+-31}
+−31	1	-1	3	L1	G_{+-31}
+−31	1	-1	3	L1	G_{+-31}
+−32	1	-1	3	L2	G_{+-32}
+−32	1	-1	3	L2	G_{+-32}
+−32	1	-1	3	L2	G_{+-32}
+−41	1	-1	4	L1	G_{+-41}
+−41	1	-1	4	L1	G_{+-41}
+−41	1	-1	4	L1	G_{+-41}
+−42	1	-1	4	L2	G_{+-42}
+−42	1	-1	4	L2	G_{+-42}
+−42	1	-1	4	L2	G_{+-42}
+−51	1	-1	5	L1	G_{+-51}
+−51	1	-1	5	L1	G_{+-51}
+−51	1	-1	5	L1	G_{+-51}
+−52	1	-1	5	L2	G_{+-52}
+−52	1	-1	5	L2	G_{+-52}
+−52	1	-1	5	L2	G_{+-52}
++11	1	1	1	L1	G_{++11}
++11	1	1	1	L1	G_{++11}
++11	1	1	1	L1	G_{++11}
++12	1	1	1	L2	G_{++12}
++12	1	1	1	L2	G_{++12}
++12	1	1	1	L2	G_{++12}
++21	1	1	2	L1	G_{++21}
++21	1	1	2	L1	G_{++21}
++21	1	1	2	L1	G_{++21}
++22	1	1	2	L2	G_{++22}
++22	1	1	2	L2	G_{++22}
++22	1	1	2	L2	G_{++22}
++31	1	1	3	L1	G_{++31}
++31	1	1	3	L1	G_{++31}
++31	1	1	3	L1	G_{++31}
++32	1	1	3	L2	G_{++32}
++32	1	1	3	L2	G_{++32}
++32	1	1	3	L2	G_{++32}
++41	1	1	4	L1	G_{++41}
++41	1	1	4	L1	G_{++41}
++41	1	1	4	L1	G_{++41}
++42	1	1	4	L2	G_{++42}
++42	1	1	4	L2	G_{++42}
++42	1	1	4	L2	G_{++42}
++51	1	1	5	L1	G_{++51}
++51	1	1	5	L1	G_{++51}
++51	1	1	5	L1	G_{++51}
++52	1	1	5	L2	G_{++52}
++52	1	1	5	L2	G_{++52}
++52	1	1	5	L2	G_{++52}

Appendix B: Gain Measurements

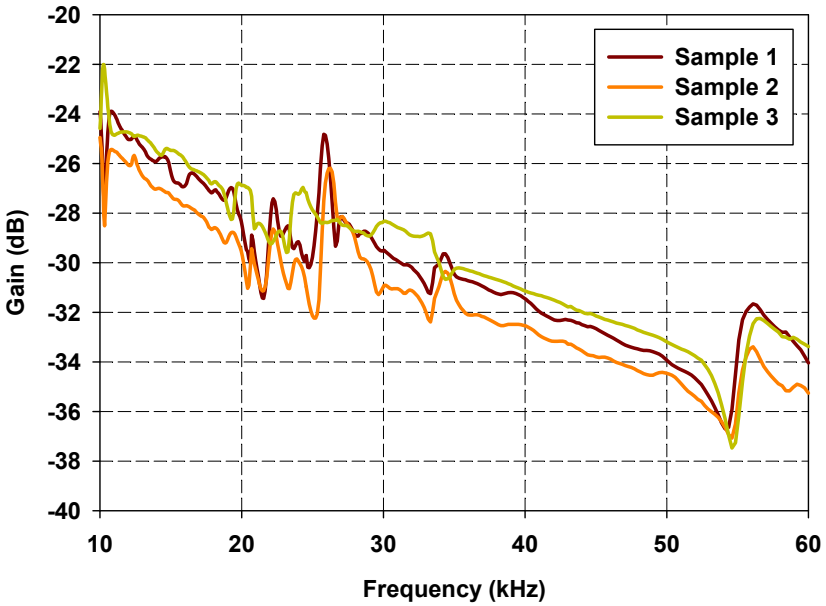

Typical Gain measurement of sample: 300 mm^2, Cu-Ni and thickness 110µm, weight: 20 grams

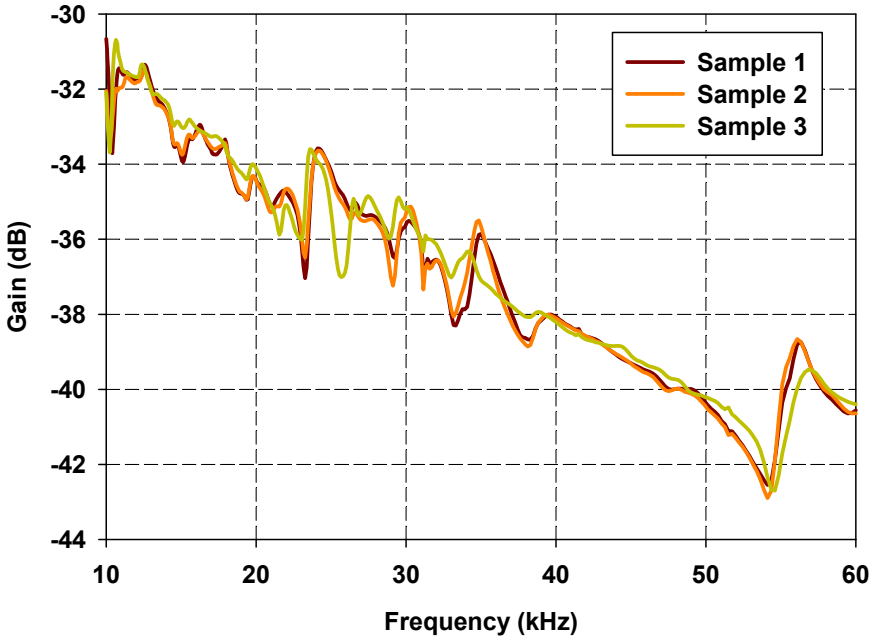

Typical Gain measurement of sample: 300 mm^2, Cu-Ni and thickness 110µm, weight: 50 grams

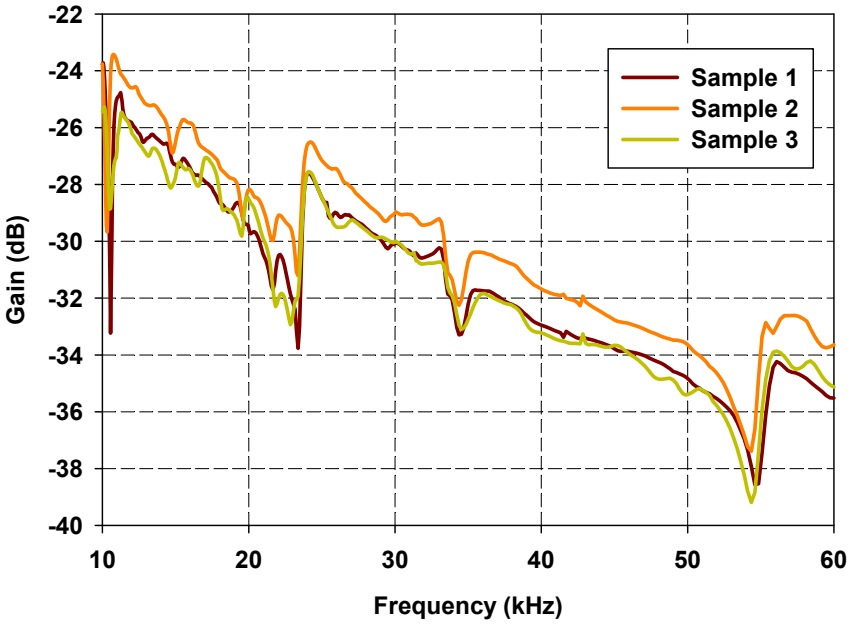

Typical Gain measurement of sample: 150 mm^2, Cu-Ni and thickness 110µm, weight: 50 grams

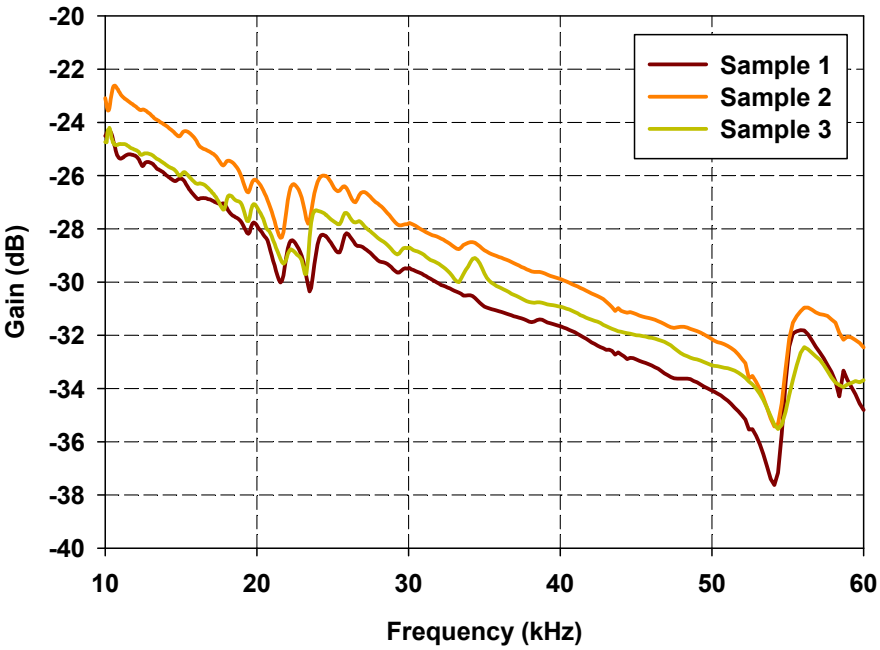

Typical Gain measurement of sample: 300 mm^2, Ag and thickness 110µm, weight: 20 grams

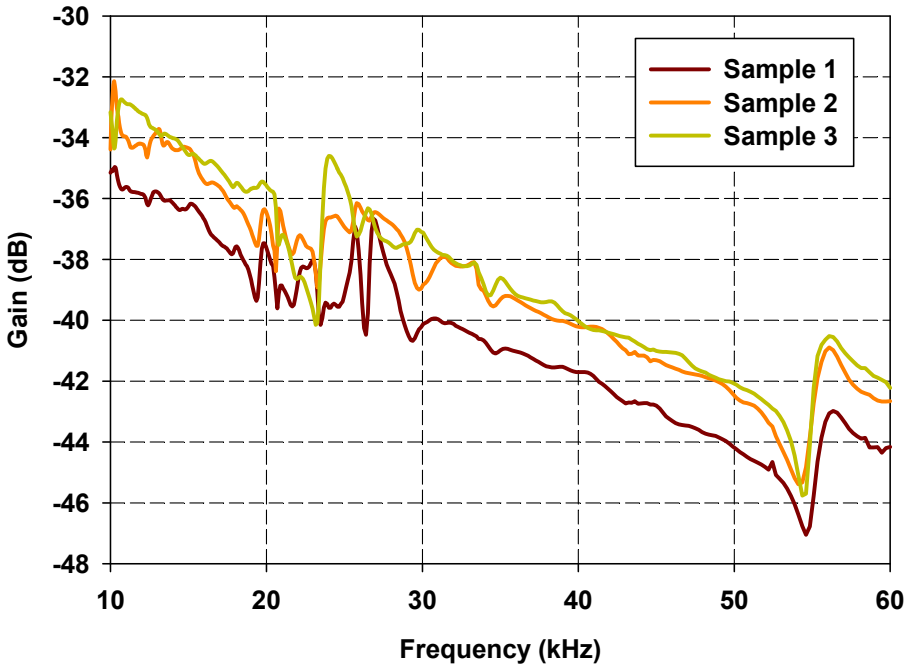

Typical Gain measurement of sample: 300 mm^2, Cu-Ni and thickness 28µm, weight: 20 grams

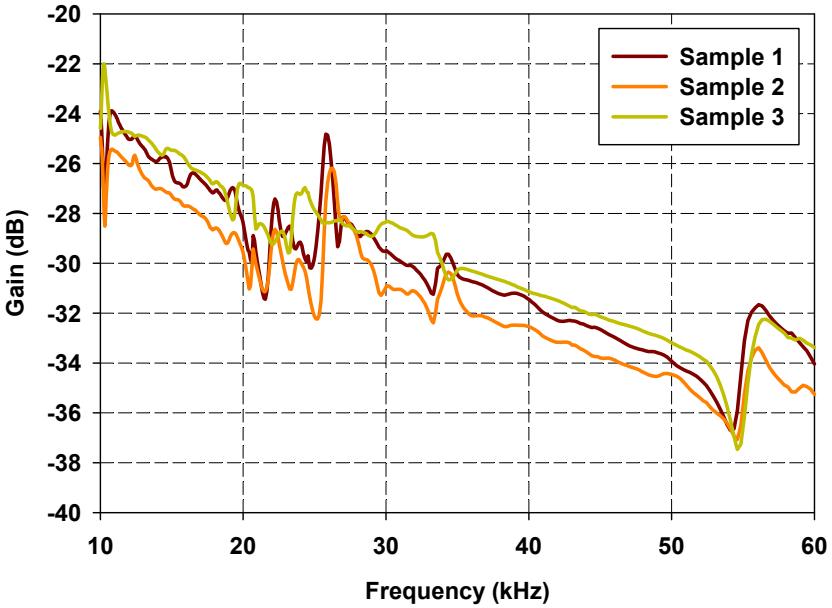

Typical Gain measurement of sample: 300 mm^2, Cu-Ni and thickness 110µm, weight: 20 grams

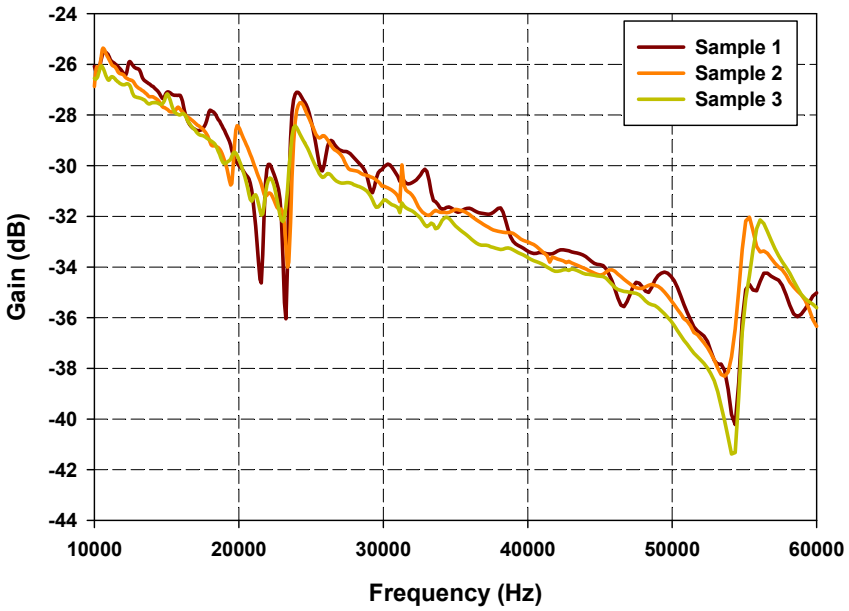

Typical Gain measurement of sample: 196 mm^2, Ag and thickness 110µm, weight: 50 grams

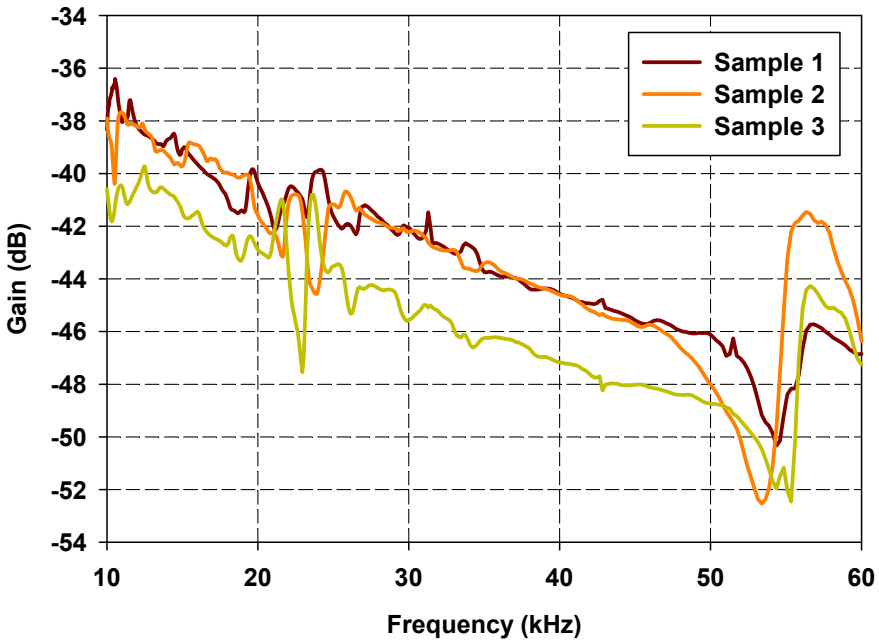

Typical Gain measurement of sample: 196 mm^2, Cu-Ni and thickness 28µm, weight: 50 grams

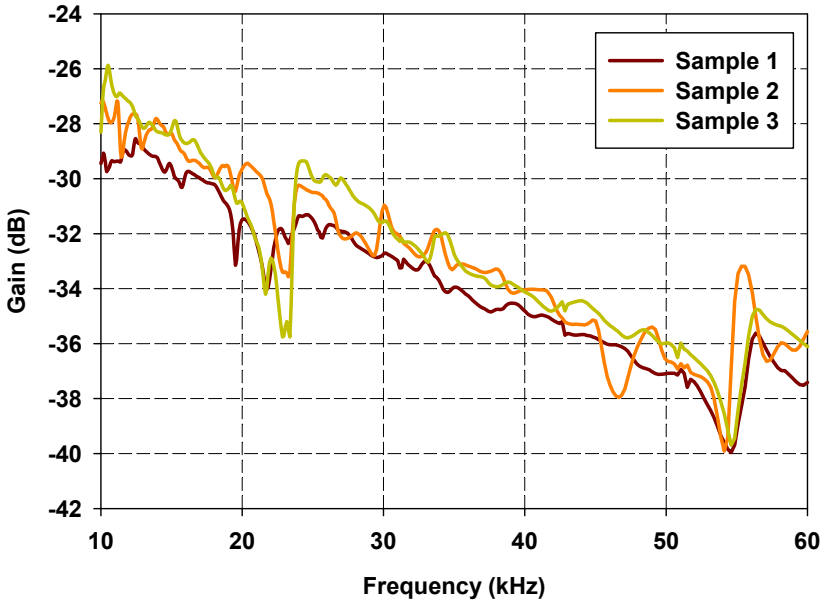

Typical Gain measurement of sample: 196 mm^2, Cu-Ni and thickness 110µm, weight: 50 grams

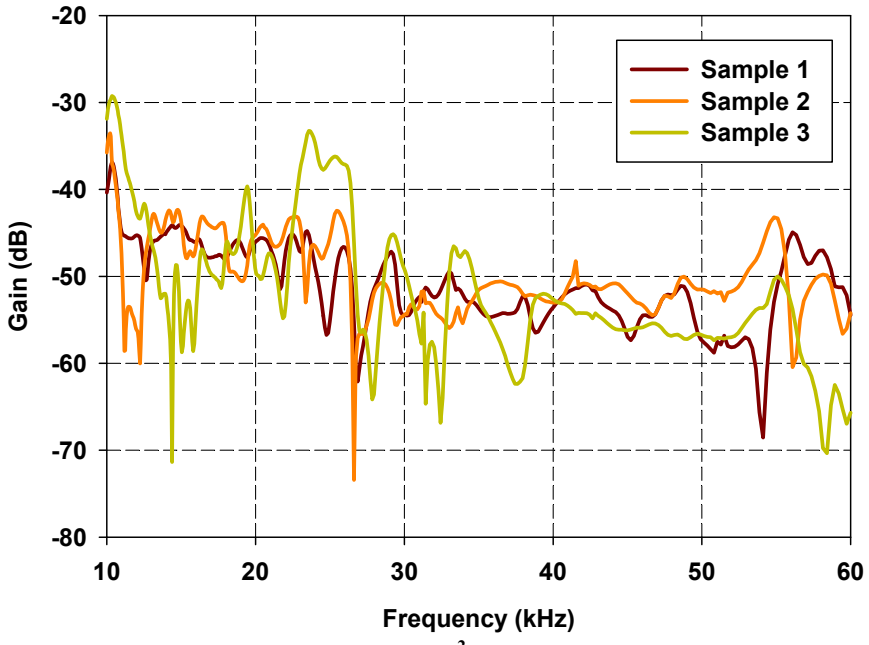

Typical Gain measurement of sample: 300 mm^2, Ag and thickness 110µm, weight: 50 grams

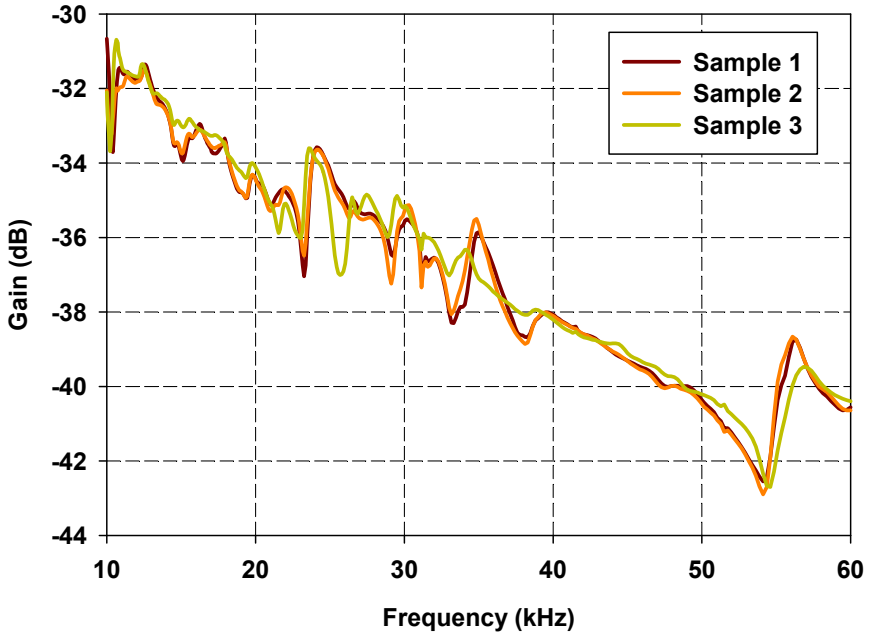

Typical Gain measurement of sample: 300 mm^2, Cu-Ni and thickness 110µm, weight: 50 grams

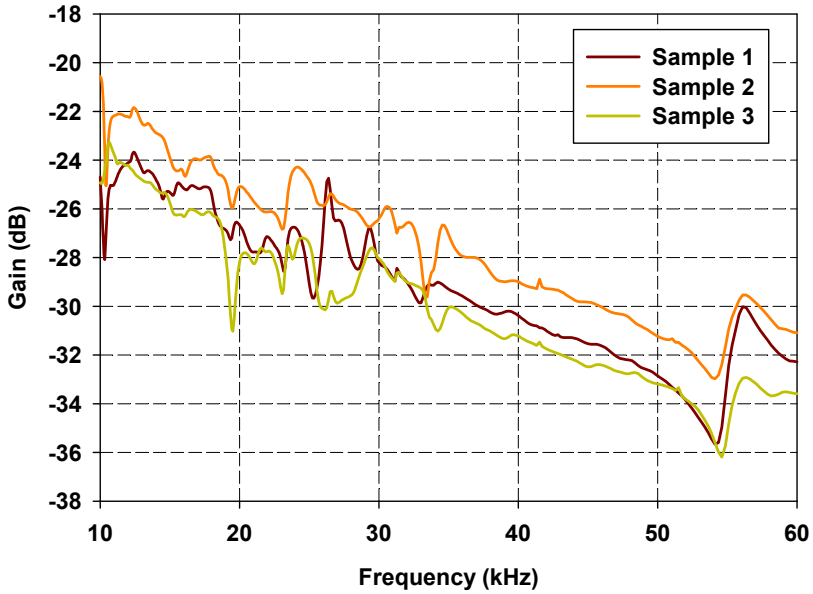

Typical Gain measurement of sample: 300 mm^2, Cu-Ni and thickness 28µm, weight: 50 grams

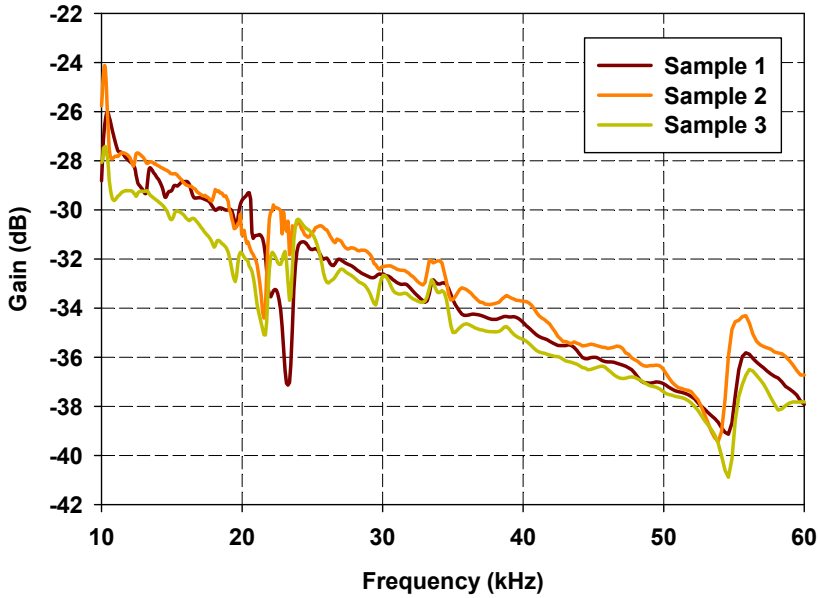

Typical Gain measurement of sample: 150 mm^2, Ag and thickness 110µm, weight: 20 grams

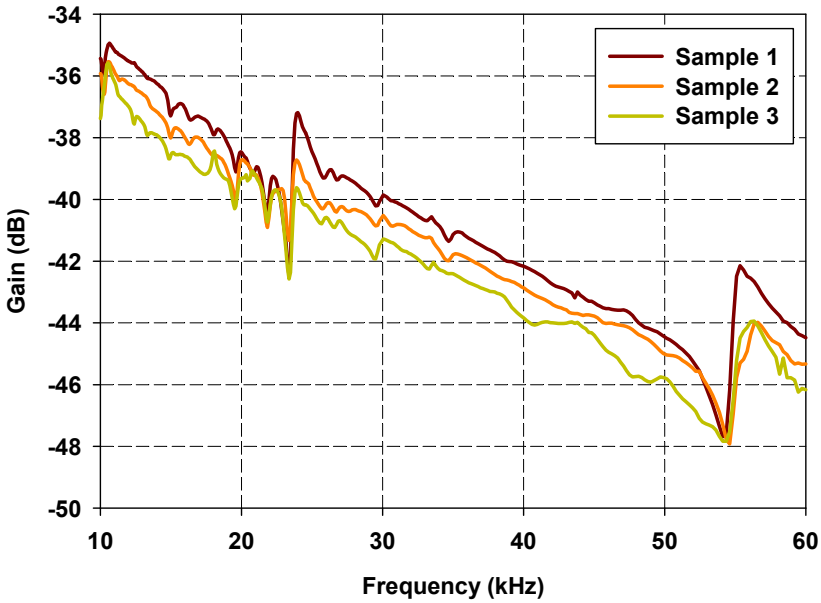

Typical Gain measurement of sample: 150 mm^2, Cu-Ni and thickness 28µm, weight: 20 grams

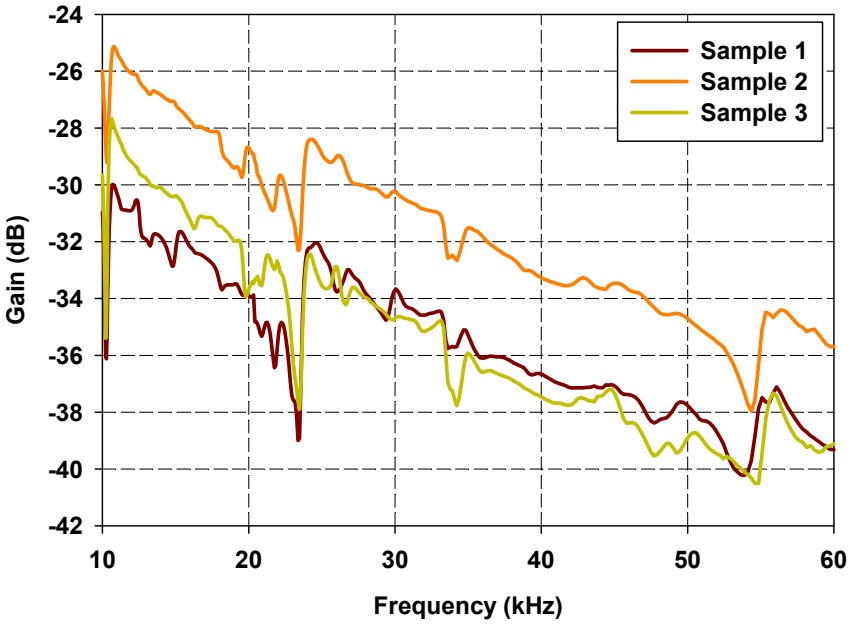

Typical Gain measurement of sample: 150 mm^2, Cu-Ni and thickness 110µm, weight: 20 grams

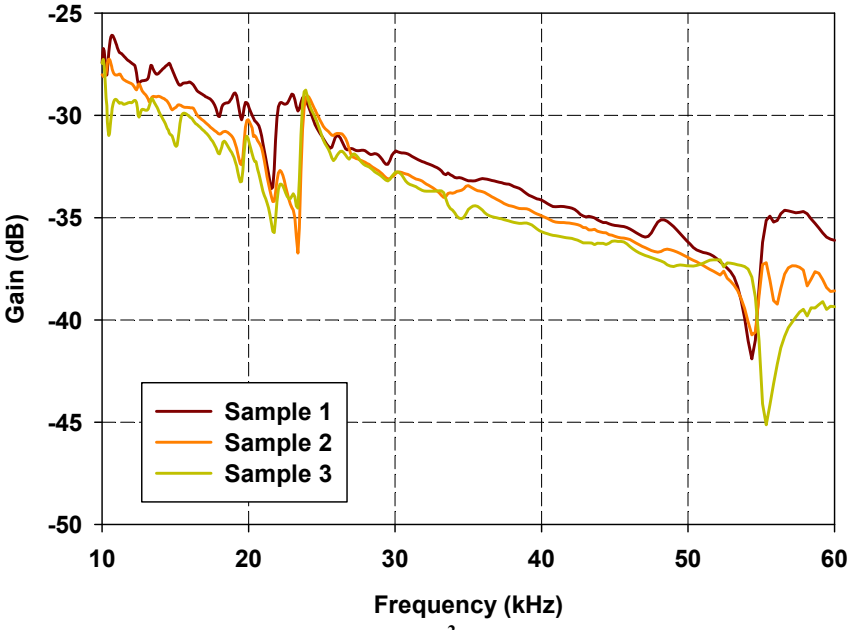

Typical Gain measurement of sample: 196 mm^2, Ag and thickness 110µm, weight: 20 grams

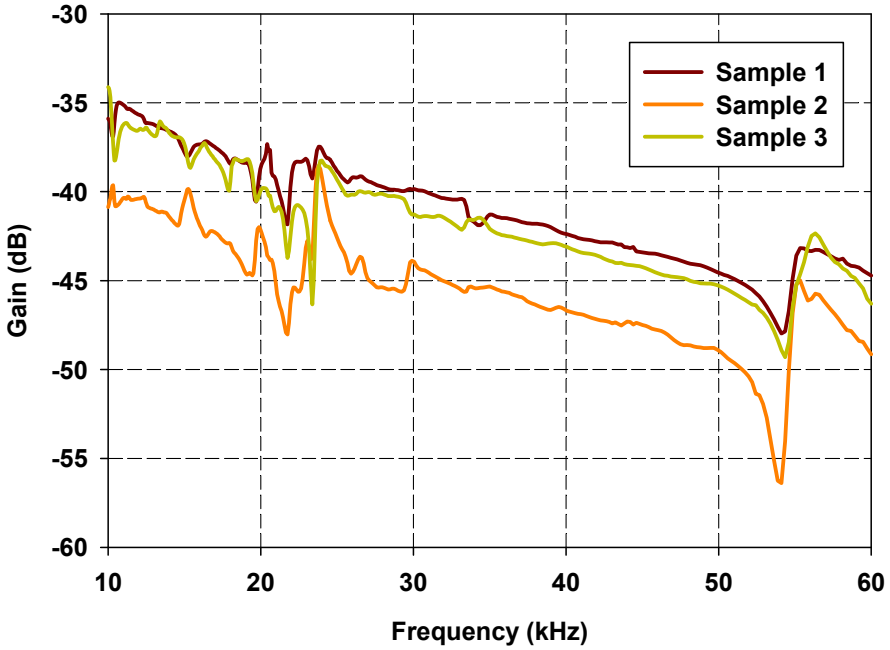

Typical Gain measurement of sample: 196 mm^2, Cu-Ni and thickness 28µm, weight: 20 grams

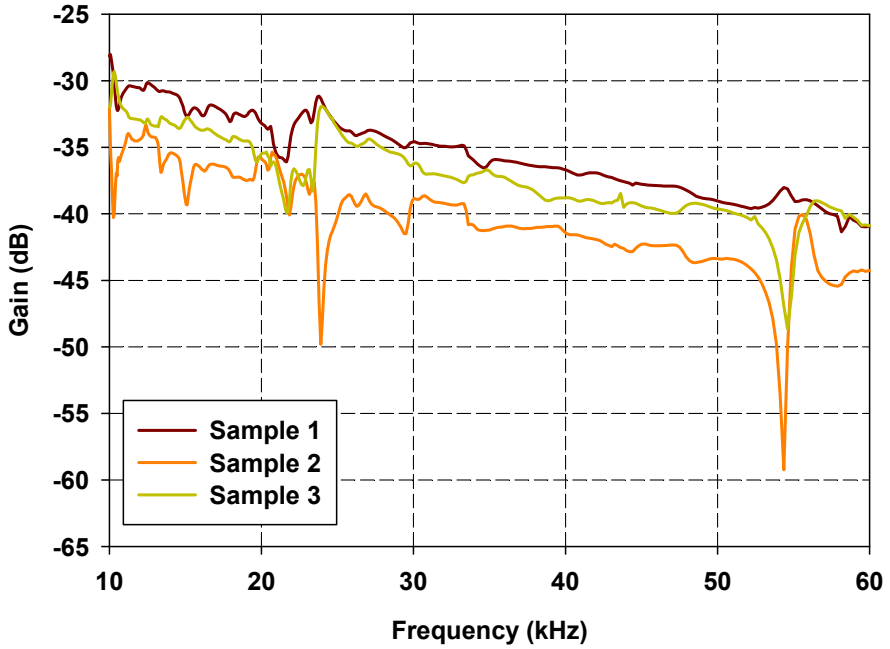

Typical Gain measurement of sample: 196mm^2, Cu-Ni and thickness 110µm, weight: 20 grams

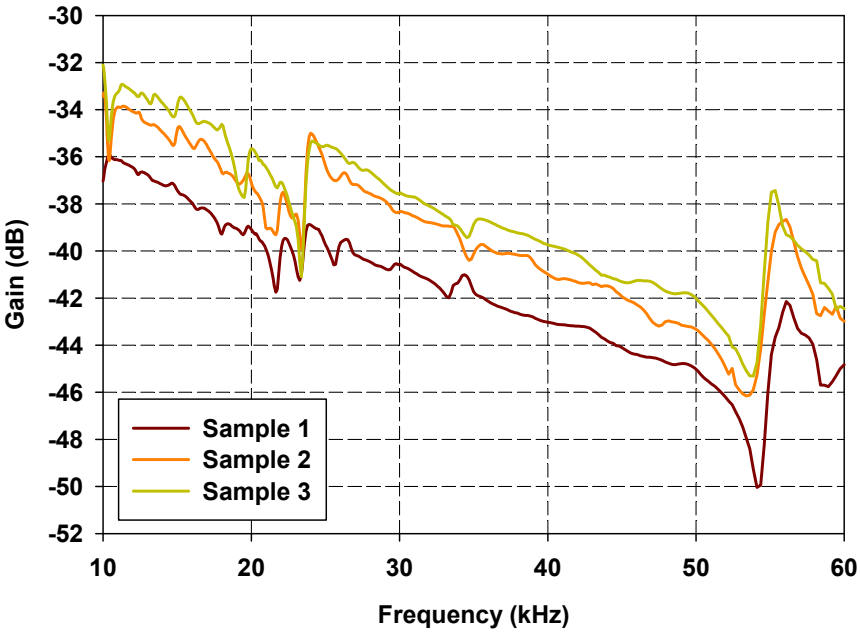

Typical Gain measurement of sample: 225 mm^2, Ag and thickness 28µm, weight: 20 grams

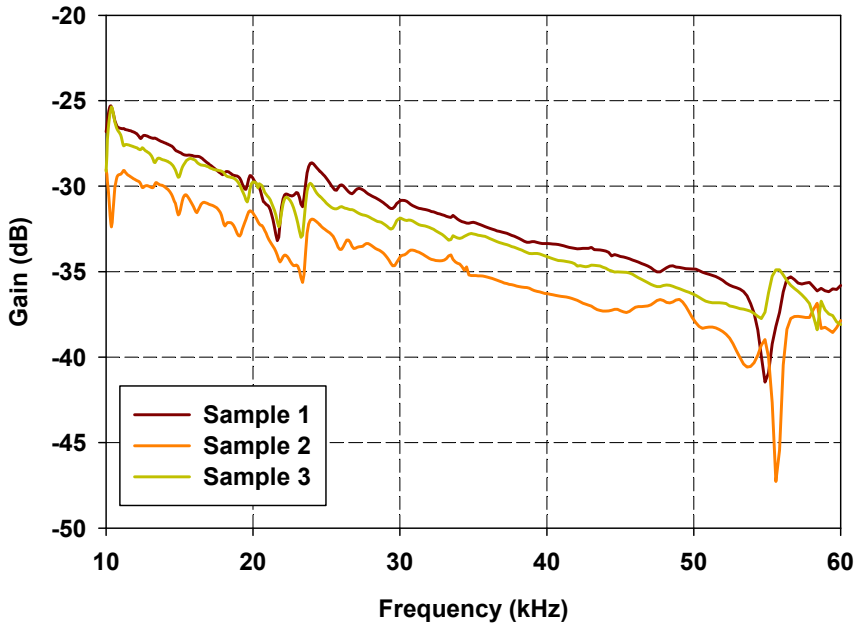

Typical Gain measurement of sample: 225 mm^2, Ag and thickness 110µm, weight: 20 grams

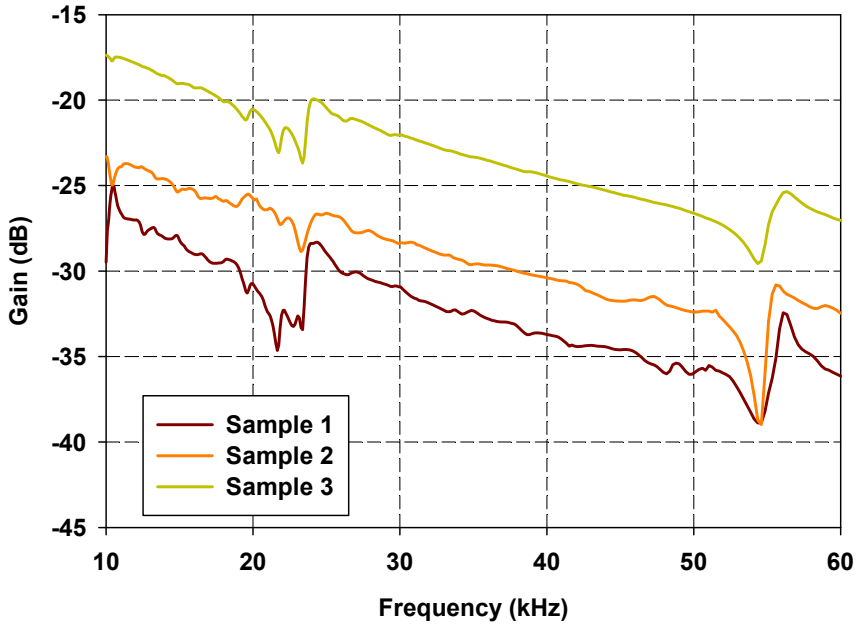

Typical Gain measurement of sample: 225 mm^2, Ag and thickness 110µm, weight: 50 grams

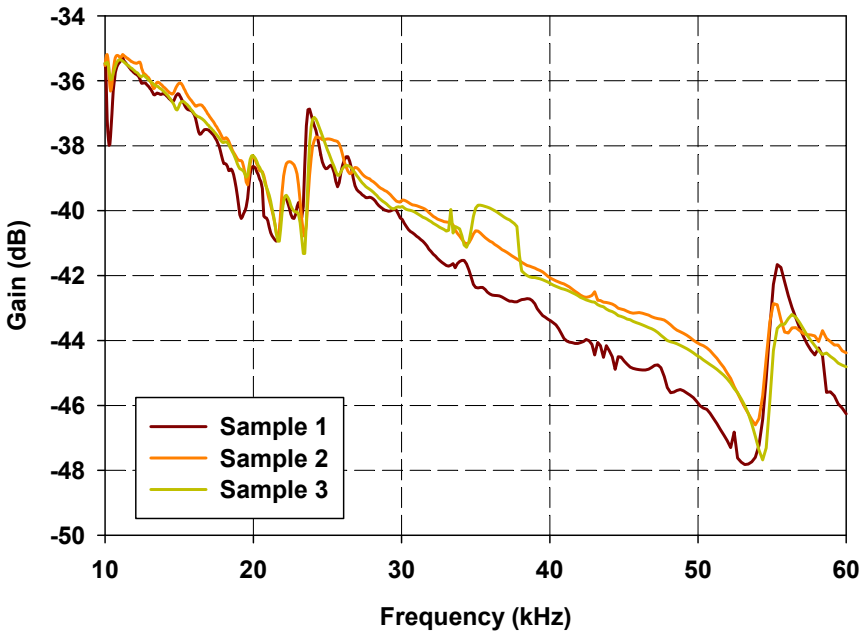

Typical Gain measurement of sample: 225 mm^2, Cu-Ni and thickness 28µm, weight: 20 grams

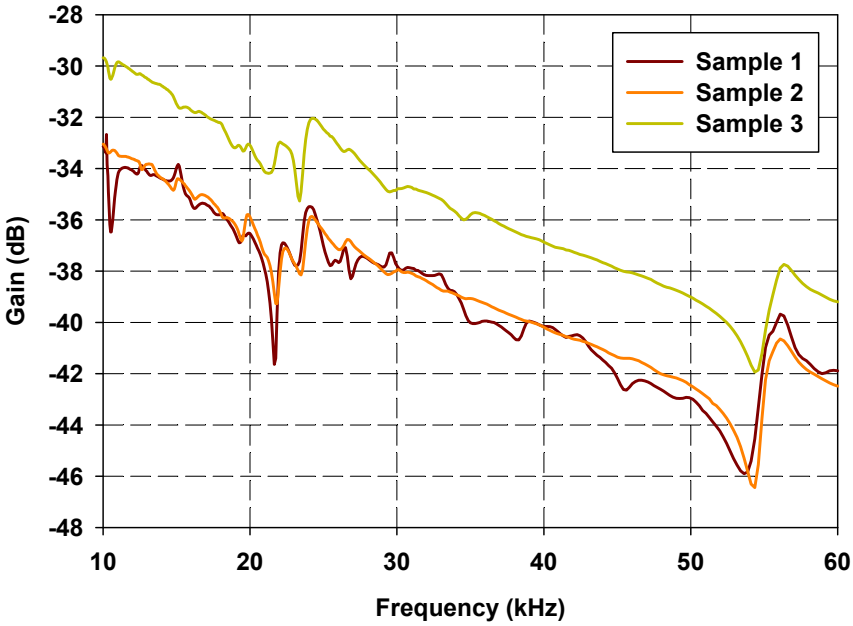

Typical Gain measurement of sample: 225 mm^2, Cu-Ni and thickness 28µm, weight: 50 grams

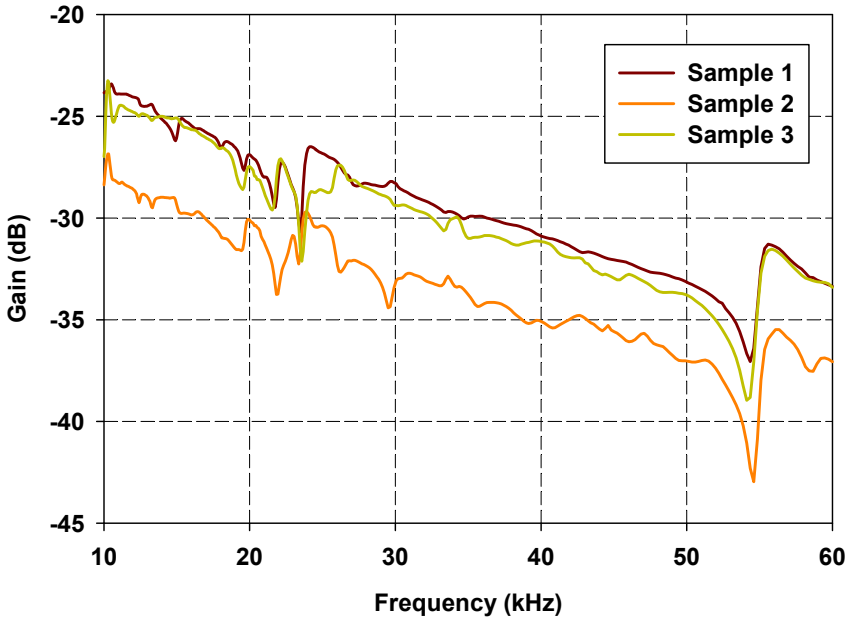

Typical Gain measurement of sample: 225 mm^2, Cu-Ni and thickness 110µm, weight: 20 grams

Appendix C: Repeatability and Reliability Measurements

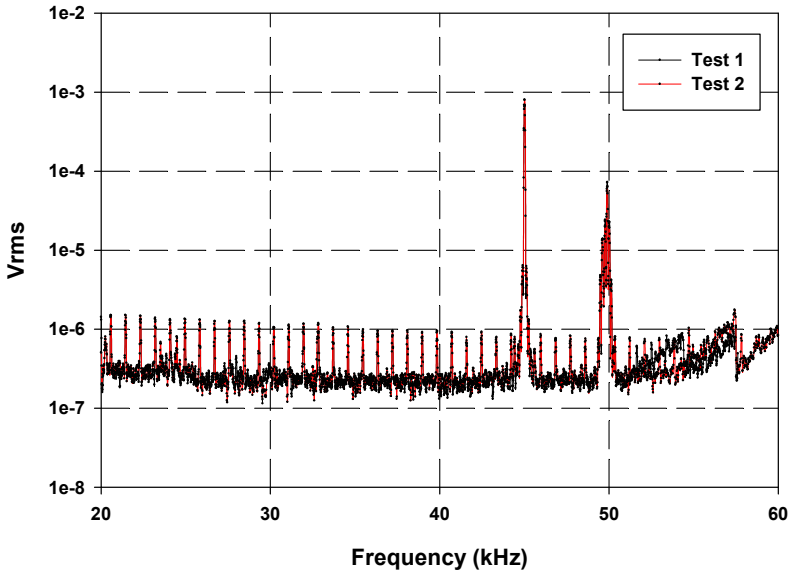

Output signal measured–subject 1, sensor 1

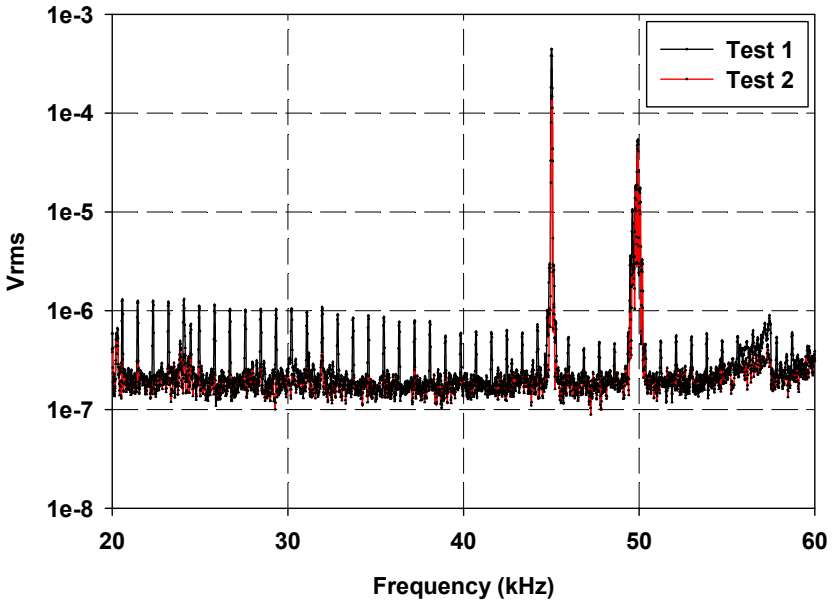

Output signal measured–subject 1, sensor 2

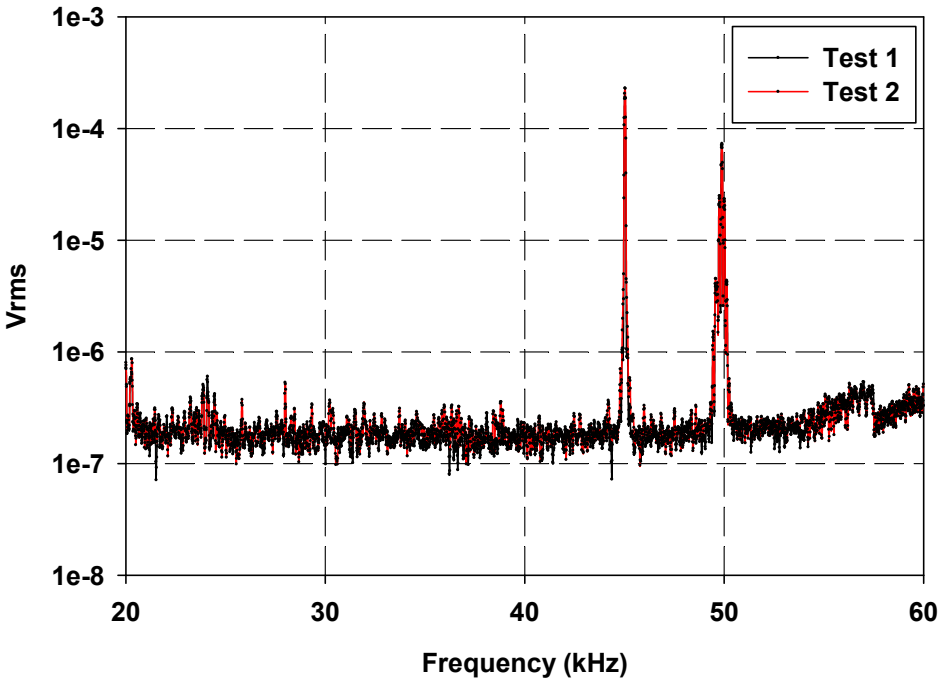

Output signal measured–subject 2, sensor 1

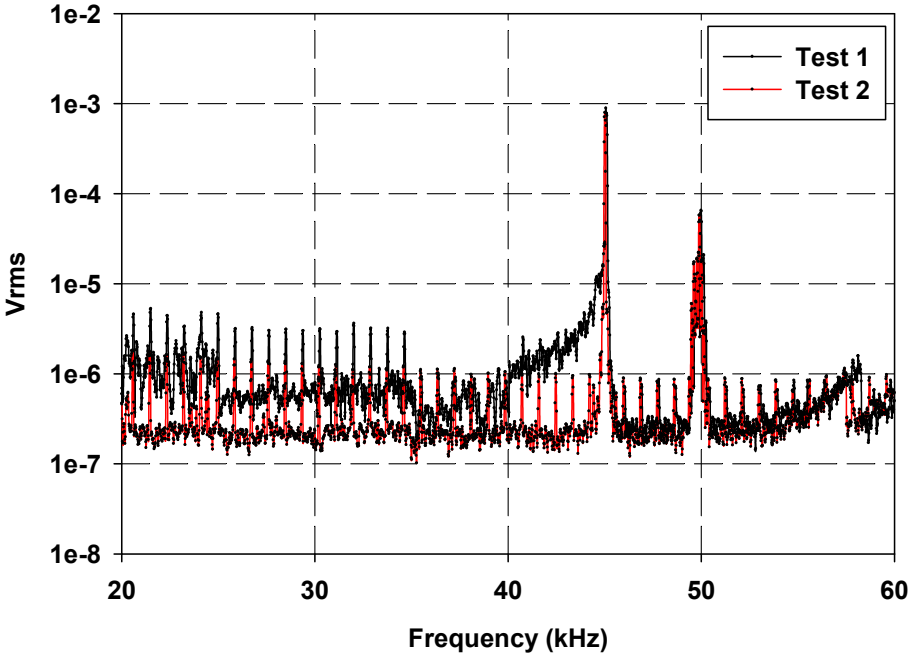

Output signal measured–subject 2, sensor 2

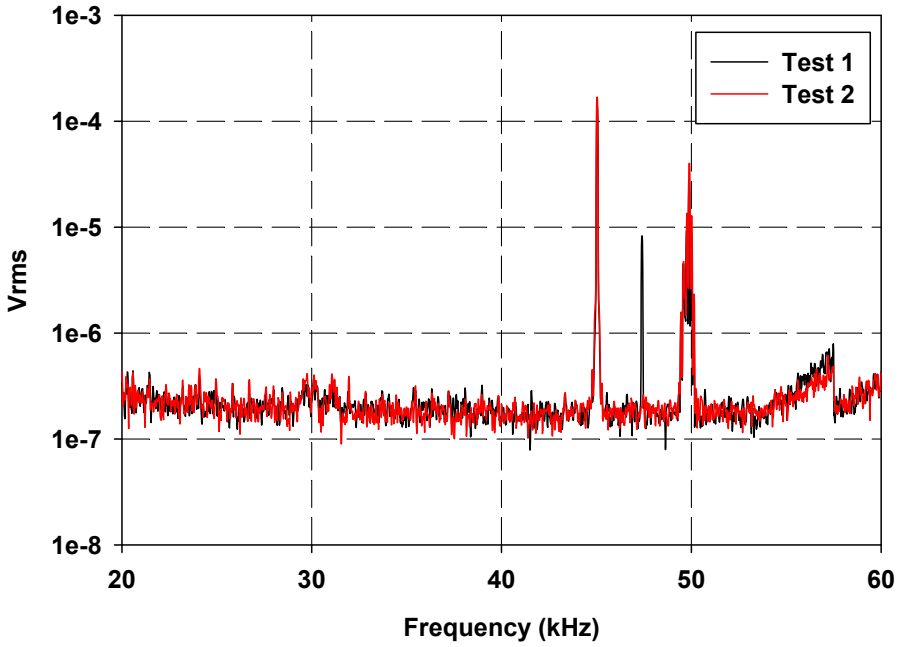

Output signal measured–subject 3, sensor 1

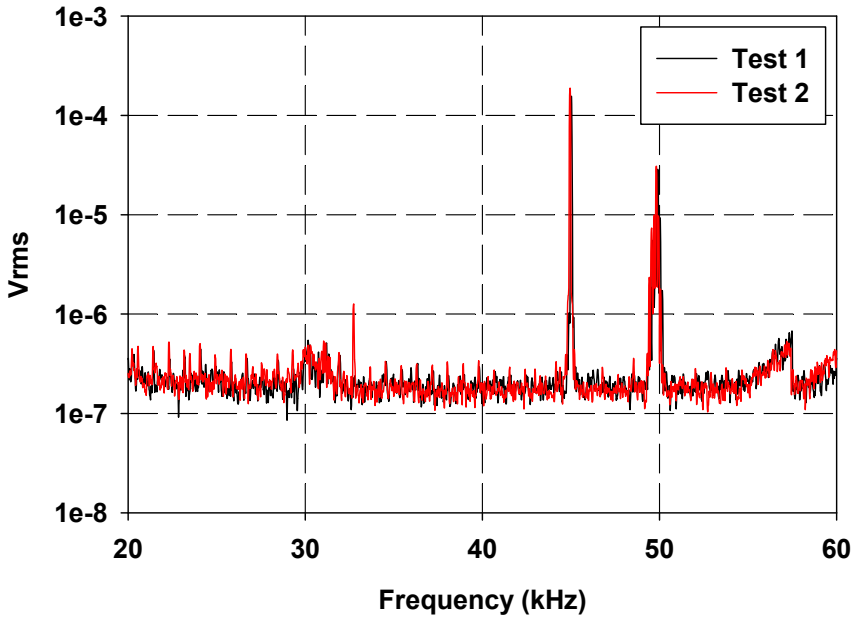

Output signal measured–subject 3, sensor 2

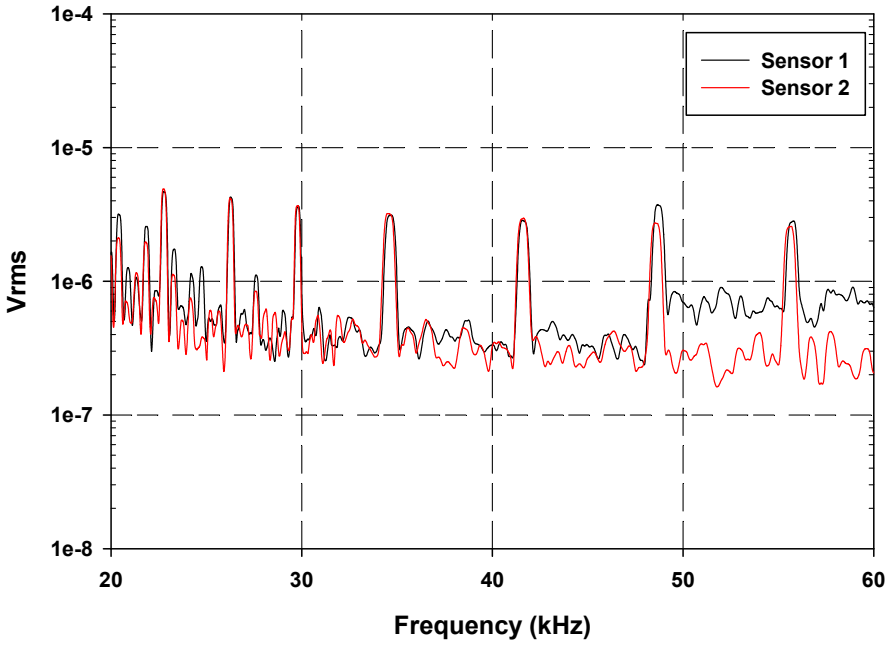

Output signal measured–subject-1, test-1

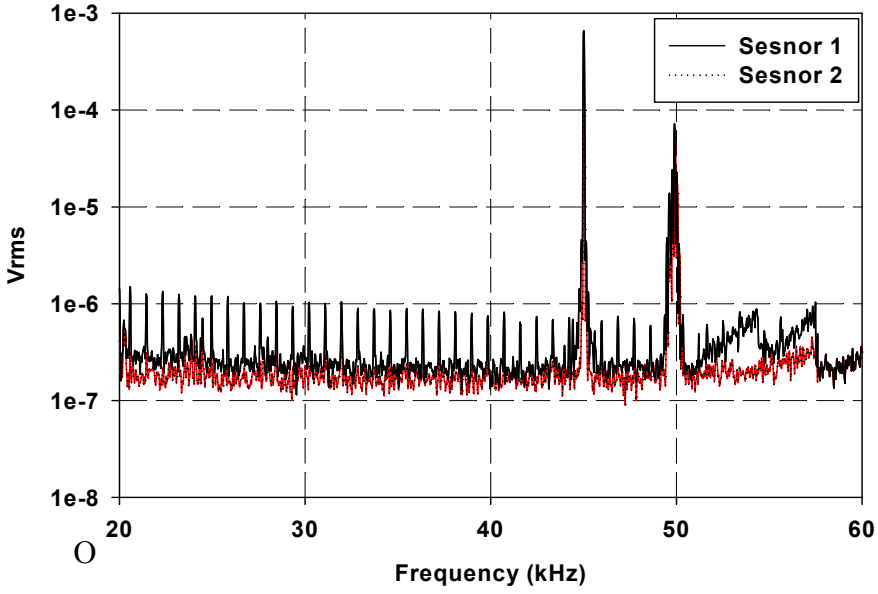

O

Output signal measured–subject-1, test-2

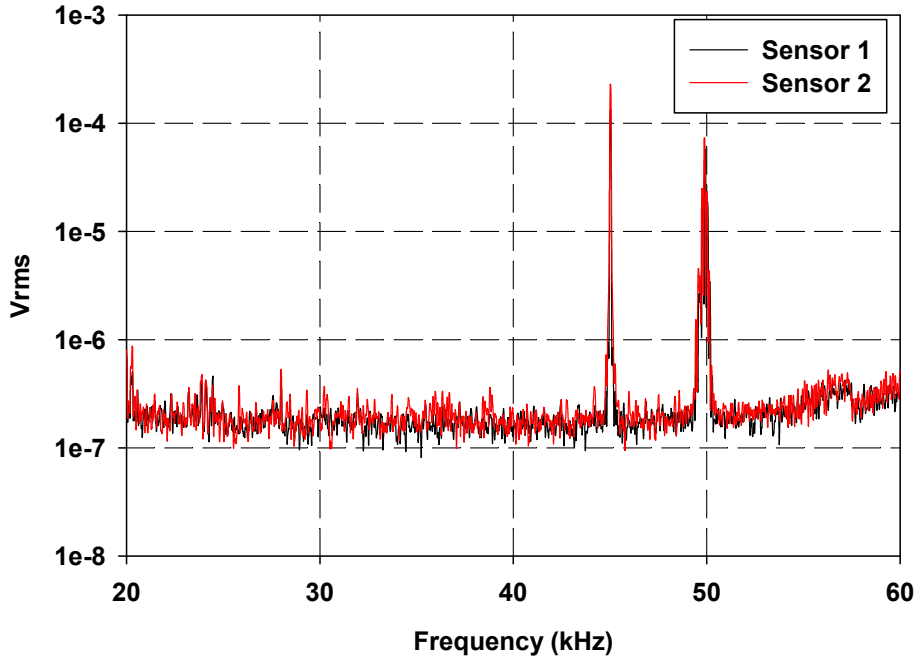

Output signal measured–subject-2, test-1

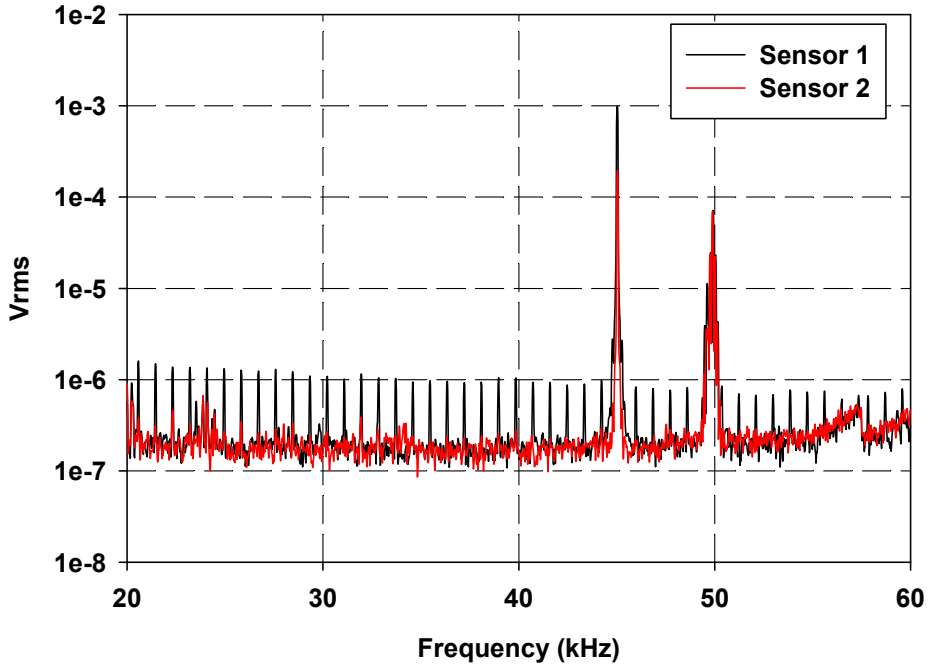

Output signal measured–subject-2, test-2

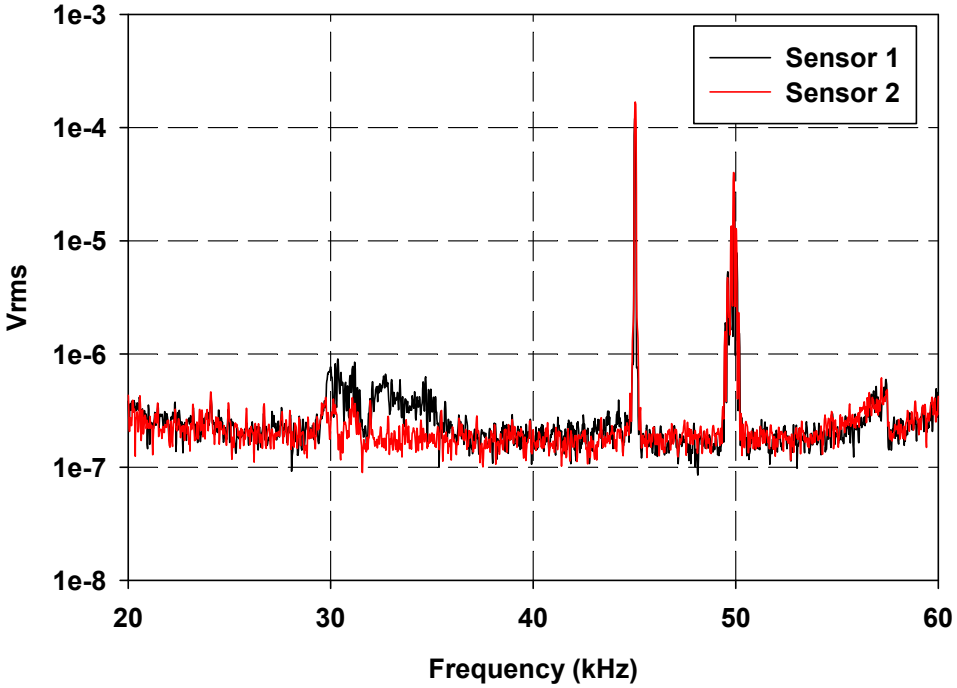

Output signal measured–subject-3, test-1

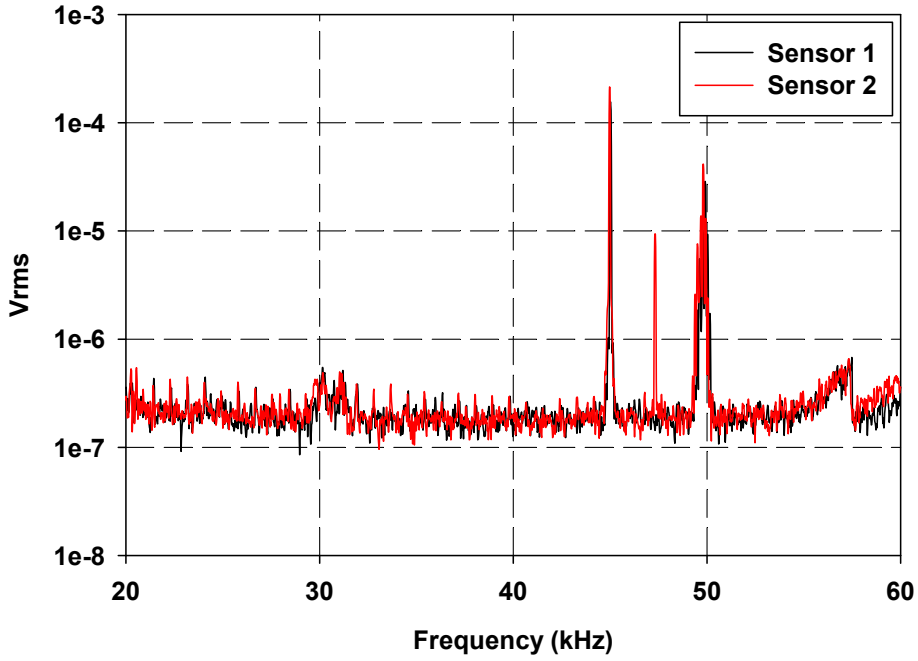

Output signal measured–subject-3, test-2

VITA

Vivek Vijaywargi was born in Hyderabad –Andhra Pradesh, India on November 14th, 1985. He attended Guru Nanak Engineering College affiliated to JNTU where he obtained a Bachelor of Technology degree in June 2007. He was the class representative of Department of Mechanical from August 2003 to May 2007. His senior design project was on the title "Automation of strip feeding, piercing and blanking operations using electro pneumatics and programmable logic controllers (PLC)". He was awarded the Graduate Teaching Assistantship Award by School of Engineering, VCU in 2007-2009 academic year. Then, while pursuing his masters degree, had assisted in classes like Statics, Kinematics and Dynamics, Solid Mechanics Laboratory as a Teaching Assistant.